STUDY OF ISOTHERMAL MULTIEXPONENTIAL TRANSIENTS FROM DEEPLEVELS IN SEMICONDUCTORS

A Thesis Submitted
In Partial Fulfilment of the Requirements
for the Degree of

MASTER OF TECHNOLOGY

by
ASHUTOSH RAZDAN

٧٤٢٨٥

to the

DEPARTMENT OF ELECTRICAL ENGINEERING
INDIAN INSTITUTE OF TECHNOLOGY, KANPUR
SEPTEMBER 1984

CERTIFICATE

This is to certify that the thesis entitled 'STUDY OF ISOTHERMAL MULTIEXPONENTIAL TRANSIENTS FROM DEEP LEVEL IMPURITIES IN SEMICONDUCTORS' is a record of work carried out by Shri Ashutosh Razdan, Roll No. 8210404 under my supervision and that it has not been submitted elsewhere for a degree.

(R. Sharan)
Professor
Department of Electrical Engineeri
Indian Institute of Technology
Kanpur

EE-1984-M-RAZ-STU

T 1984

84237

Dedicated

to

Tathaji and Amma

ACKNOWLEDGEMENTS

It is with deep sense of gratitude that I thank my guide Dr. R. Sharan for his guidance and concern at every stage of this thesis.

It is with pleasure that I thank Dr. Rakesh K. Lal for his timely help and company during the course of this work. I also thank Dr. J. Narain for his everwilling help throughout the work.

I take this opportunity to thank Research Engineers, Mr. Prem Malhotra and Mr. G.N.M. Sudhakar for their friendly help.

I thank all my colleagues in particular Capt. A.K. Das, Mr. U.K. Mukhopadhyaya and Mr. R.P. Gupta for nice company and enthusiastic help towards the last stages of this work.

Last but not the least, I acknowledge the excellent typing by Mr. J.S. Rawat.

Sept. 25,1984 - ASHUTOSH RAZDAN

ABSTRACT

This work deals with characterization of deep level impurities, particularly of Gold in silicon. Isothermal relaxation data, using space charge spectroscopic principles, has been obtained, using set ups to measure low level capacitance and current signals from the device. Both single shot and synchronous detection methods of measurement and analysis have been used. The problem of det. of multi-exponential transients, which has been eluding an accurate and reliable solution, has been treated using an appropriate signal processing algorithm. In the present work the acquisition and analysis functions, which are performed simultaneously in the classical deep level transient spectroscopy (DLTS) developed by Lang, have been separated. This separation has been achieved using transient recording and analysis on a signal analyser, whose large memory as well as facilities for development of various analysis and signal processing routines have been found of immense use in analysis The results have been obtained on a commercial $P^{+}N$ Jn diode 1N4148, for which the other relevant data was readily available. Important parameters such as activation energy and capture cross-sections have been determined.

TABLE OF CONTENTS

		Page
CHAPTER 1	INTRODUCTION	1
CHAPTER 2	ISOTHERMAL RELAXATION STUDY FOR DEEP LEVEL IMPURITIES	7
	2.1 Introduction	7
	2.2 Capacitance and current as probes to Relaxation study.	11
	2.3 Techniques used in analysis of transients	20
CHAPTER 3	TRANSIENT DATA ANALYSIS	25
	3.1 Introduction	25
	3.2 Analysis for single exponential signals	25
	3.3 Analysis for multiexponential signals	35
	3.4 Analysis for DLTS	49
CHAPTER 4	MEASUREMENT SYSTEM FOR DATA ACQUISITION	51
	4.1 Introduction	51
	4.2 Measurement system for data acquisition	51
	4.3 Design of capacitance transient measurement module	55
	4.4 Design of current transient measurement module	63
CHAPTER 5	EXPERIMENTAL RESULTS AND DISCUSSION	67
	5.1 Introduction	67
	5.2 Current transients	67
	5.3 Capacitance transients	82
CHAPTER 6	CONCLUSION	94
APPENDIX I		96
APPENDIX II		103
APPENDIX III		111
BIBLIOGRAPHY		113

CHAPTER 1

INTRODUCTION

Deep levels in semiconductors play an important role in device performance. They determine crucial device parameters as mean lifetime, activation energy, recombination efficiency etc. Hence it is essential to accurately characterize deep levels. This, however, is not a simple process, essentially because deep levels can get created not only when a known impurity is added but also they get inadvertently created due to lattice defects. The presence of one can affect the performance of the other deep levels as a recombination center. For instance Gold is extensively used in semiconductor industry for fast switching operations and lot of data on its parameters has been reported in literature. The reported values, however, vary by orders of magnitude. Wu and Peaker [16] have reported a survey of these values over the years. Table 1.1 just lists the electron cross-section values of Gold acceptor in silicon. This clearly suggests a degree of unpredictability related to values of Gold parameters. This unpredictability is partly justified by Bullis [9], wherein these parameters are found dependent upon several factors like the characteristics of initial material,

Table 1.1: Electron cross-section of Gold acceptor in silicon.

Author	Year	$\sigma_n(cm^2)$	Temp(K)	Material	Technique
Bemski and Struthers	1958	5×10^{-16}	200-450	$N_T=N_D$	Minority Lifetime
Davies	1959	2×10^{-15}	77	CZ $N_T>>N_D$	Majority Lifetime
Fairfield and Gokhale	1965	8.4×10^{-17}	300	CZ $N_T=0.1$ N_D	P.C. Decay
Senechal and Basinski	1968	2.5×10^{-15}	250	CZ $N_T=N_D$	Junc. Cap.
Sah et.al.	1970	2×10^{-16}	80	$N_T=0.3N_D$	Maj. Flux junc. cap.
Zohta	1972	4.6×10^{-15}	300	FZ $N_T=N_D$	Junc. Cap.
Kassing and Lenz	1974	8.3×10^{-15}	300	n^+i $n^+N_T>N_D$	SCLC
Pals	1974	1.3×10^{-16}	77-220	CZ $N_T=0.2$ N_D	Pulse/Junc. cap.
Nagasawa and Schultz	1975	2.2×10^{-15}	300	Implanted	Pulse/Junc. Cap.
Kassing et.al.	1975	7.3×10^{-14}	172-316	n^+i $n^+N_T>N_D$	SCLC
Barbolla et.al.	1976	8.3×10^{-17}	80-205	CZ $N_T=0.3$ N_D	Pulse/Junc. Cap.
Dudeck and Kassing	1977	1.5×10^{-15}	300	n^+i $n^+N_T>N_D$	SCLC
Brotherton and Bicknall	1978	9.10^{-17}	77-280	CZ $N_T=0.1N_D$	Pulse/Junc.Ca
Nassibian and Farone	1978	1.10^{-15}	235-265		Minority/life
Lang et.al	1980	6.9×10^{-17}	295	EPI $N_T<0.1N_D$	Pulse/Junc.Ca
Lang et.al.	1980	1.7×10^{-16}	115-424	CZ $N_T=0.1N_D$	Pulse/Junc.ca
Wu and Peaker	1981	8.5×10^{-17}	80-200	CZ N_T $0.1N_D$	Pulse/Junc.ca

behaviour of one type of deep level in presence of another deep level or even the shallow levels. Lang [10]has conclude that in place of a well defined unique level, there are family o closely related but different gold based complexes.

This work concentrates on Gold in silicon. The deep level impurity characterization can be done using either isothermal or nonisothermal relaxation. Here the former method is chosen and in particular, junction spectroscopic methods have been used. These methods have the advantage that one can distinguish between electron and hole traps and further one can get directly, emission rates and related data. Both single shot and synchronous methods of analyses have been used. They are detailed in Chapter 2. Chapter 2 also includes the theory behind current and capacitance transients as tools to deep level characterization using isothermal junction transient methods. Lang's method of Deep Level Transient spectroscopy (DLTS) is also explained in Chapter 2.

Chapter 3 discusses the analysis procedures for current and capacitance transients from the sample. It is found that this data is quite unamenable to accurate characterization because of two reasons, one that the transient has a steady state level on which it sits and two,

that instead of having single exponent, it can have a sum of exponents (or multiexponent). Physically multiexponents can mean that more than one trap are involved in recombination process. The data in that case can be thought of having form like $\sum_{i=1}^{n} A_i e^{-\alpha_i t}$. The problem is to accurately find values of A_i, n and α_i. Apparently it looks a trivial problem, which it is not [11]. According to Lanczos [11], the practical solution of these problems is beset with numerical difficulties. For an accurate determination, large data accuracy is needed. If it is not so, one can get totally unsatisfactory results. In no way, any of the least square treatments can help retrieve the situation for insufficiently accurate initial data. Chapter 3 goes into details of these problems. Multiexponents have been extracted using an appropriate signal processing algorithm due to Gardner et.al. [12]. Chapter three contains the details of this method and the reasons of its success. In the same chapter, several other signal analysing algorithms are described. They deal with the determination of parameters in a single exponential decay from the samples, in the presence of a constant d.c. shift.

The particular method of DLTS suffers from the fact that analysis is done using

hardwired instruments and each point in Arrhenius plot requires one thermal scan. Obviously this is very time consuming and hence this work delineates it into two independent functions of acquisition and analysis. The details of Box-car programs in Appendix I,help in underlining the advantage of using one thermal scan and getting all what one could get from conventional DLTS.

Chapter 4 contains the details of measurement system used for characterizing the deep levels. The design of capacitance and current transient measurement modules is described in the same chapter. In both the cases, the signal is of low level in nature. The capacitance transient is, in particular, monitored by high frequency small signals.

Chapter 5 contains the experimental data taken on a commercial $P^{+}N$ junction diode 1N4148. Using the theory and analyses of second and third chapters, deep level parameters like activation energy and capture cross-section have been determined. Discussions of the results follow in the same chapter.

Chapter 6 contains the conclusion and suggestions for further improvements.

Appendix I and II contain program listings for analysis procedures described in Chapter 3.

As lot of data has been obtained from the signal analyser, a typical plot is explained briefly in Appendix III.

CHAPTER 2

ISOTHERMAL RELAXATION STUDY FOR DEEP LEVEL IMPURITIES

2.1 INTRODUCTION:

Current transport in semiconductors is determined by electrons and holes in conduction and valence bands respectively. The number of electrons in the conduction band or holes in the valence band is dependent upon the doping and the generation-recombination process in the semiconductor. At any instant these carriers can be generated either thermally or by any other external perturbation and they recombine with a mean life time. The process of recombination, particularly, is strongly dependent upon the impurities in the semiconductor. Hence efforts have been made to measure the parameters of the impurities (e.g. life time etc.) accurately and relate them to various device parameters like conductivity etc. The process of recombination can be band-to-band or band-to-impurity-to band. However theoretical values assuming only band to band transitions have been orders of magnitude different from experimental results in silicon and Germanium. Shockley et.al. [6] in their theory called SRH statistics explain the discrepancy in these 'indirect' materials by assuming the existence of one or

more deep levels within the band gap. These levels act as recombination centres. Though this idea of the existence of deep levels in SRH statistics was a theoretical construct, subsequent experimentation has confirmed their presence. Thus an accurate characterization of these deep levels has helped solve two problems. One that the above said discrepancy in values of mean lifetime has been explained and secondly one can tailor device characteristics according to one's needs. The exact effect of deep levels on recombination can be known from SRH statistics. Here only those aspects of SRH statistics will be discussed which are pertinent to our characterization of deep levels.

Consider a deep level acting as a recombination center within the band gap as shown in Fig. 2.1. The deep level recombination center or trap can essentially:

1. capture electrons from conduction band r_a
2. emit electrons to conduction band r_b
3. capture holes from valence band r_c
4. emit holes to valence band r_d.

Let $\langle V \rangle$ be the mean thermal velocity

σ_n, σ_p capture cross-sections for electrons and holes

N_t the trap concentration

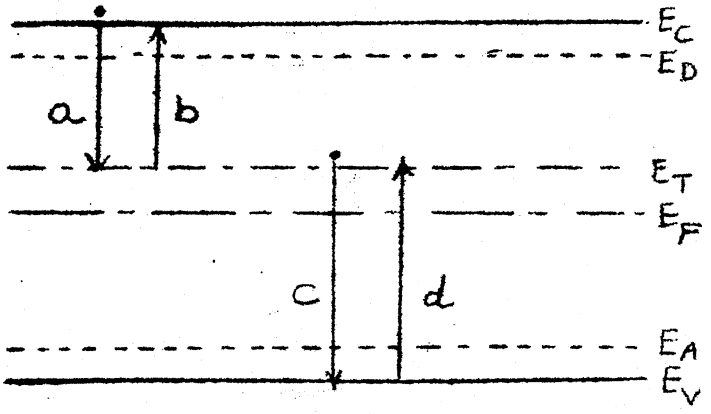

Fig. 2.1: Energy band diagram with a single trap level at E_T.

e_n, e_p the emission rates of electrons and holes and

$f = \frac{1}{1+e^{(E_t-E_F)/kT}}$ be the probability that a given trap level is occupied by an electron.

The rates of the above four processes r_a, r_b, r_c and r_d is given by

1. $r_a = \langle V \rangle \sigma_n n . N_t (1-f)$ (2.1)

2. $r_b = e_n . N_t . f$ (2.2)

3. $r_c = \langle V \rangle \sigma_p . p . N_t . f$ (2.3)

4. $r_d = e_p . N_t (1-f)$ (2.4)

under thermal equilibrium

$$r_a = r_b \text{ and } r_c = r_d$$

From $r_a = r_b$ we have from eqn. (2.1) and (2.2)

$$\langle V \rangle \sigma_n . n . N_t (1-f) = e_n N_t . f \tag{2.5}$$

on solving eqn. (2.5) one gets for e_n

$$e_n = \langle V \rangle \sigma_n N_c e^{(E_t-E_c)/kT} \tag{2.6}$$

similarly from $r_c = r_d$ one gets

$$e_p = \langle V \rangle \sigma_p N_v e^{(E_v-E_t)/kT} \tag{2.7}$$

From eqns. (2.6) or (2.7), if one plots natural logarithm of e_n or e_p against $1/T$, the resulting straight line gives the activation energy as slope and ordinate intercept provides capture cross-section. Such a plot called Arrhenius plot is used to characterize the deep level recombination centre. Hence methods, both direct and indirect, have been devised to get values of e_n or e_p. In this analysis direct method using junction spectroscopic principles has been utilized. It has been found that the capacitance or current due to the deep level filling or emptying in the space-charge region is in the form of a transient and is related to emission rates of carriers and the trap concentration. Section 2.2 gives in detail the origin of the capacitance and current transients. The analysis of these transients can be done in several ways and are detailed in Section 2.3.

2.2 CAPACITANCE AND CURRENT TRANSIENTS AS PROBES TO RELAXATION STUDY:

Let n_T and p_T be the concentration of electrons and holes at the trap. From eqn. (2.1) and (2.2), the rate of change of electron concentration $(\frac{dn}{dt})_T$ in conduction band due to trap can be found as

$$\left(\frac{dn}{dt}\right)_T = r_b - r_a = e_n n_t - c_n n p_T \qquad (2.8)$$

where $c_n = \langle V \rangle \sigma_n$

Similarly from eqns. (2.3) and (2.4), for rate of change of hole concentration $(\frac{dp}{dt})_T$ in valence band due to trap, can be written as:

$$\left(\frac{dp}{dt} \right)_T = r_d - r_c = e_p p_T - C_p\, p\, n_T \qquad (2.9)$$

From eqns. (2.1), (2.2), (2.3) and (2.4), the rate of change of trap electron concentration $(\frac{dn_T}{dt})$ is as

$$\left(\frac{dn_T}{dt}\right) = r_a - r_b + r_d - r_c$$

$$= -(e_n + c_p p + c_n n + e_p) n_T$$

$$+ (e_p + c_n n) N_{TT} \qquad (2.10)$$

where $N_{TT} = n_T + p_T$ = trap concentration. Solution of eqn. (2.10) yields within depletion region for n=p=o

$$n_T(t) = n_T(\infty) + [n_T(o) - n_T(\infty)] e^{-t/\tau_{ON}} \qquad (2.11)$$

where,

$$\tau_{ON} = \frac{1}{e_n + e_p}$$

$n_T(\infty)$ is the final value and is given by

$$n_T(\infty) = N_{TT} \left(\frac{e_p}{e_n + e_p} \right) \qquad (2.12)$$

and $$n_T(o) = N_{TT}\left(\frac{N_E}{N_E+e_1}\right) \qquad (2.13)$$

$$= N_{TT}\,(P^+N\ Jn)$$

$$= 0 \quad (N^+P\ Jn)$$

where N_E is the equilibrium concentration. From eqn. (2.11) one sees that trapped electron concentration decreases exponentially with time and hence within deplection region, the corresponding capacitance and current, too, will change according to trapped electron concentration.

A typical experiment to measure this capacitance or current transient involves application of a suitable voltage and observing the sample response. The response, however, is strongly dependent upon temperature. Therefore one does the experiment either at a constant temperature and hence isothermal measurements, or varies temperature according to a program and therefore nonisothermal measurements. This work uses isothermal conditions and the applied voltage is in the form of a pulse-bias. There are two types of pulses one can use. In one there is no carrier injection process in the sample and in another there is carrier injection. The former is called a majority carrier pulse while the latter is called minority carrier pulse. Each of

the pulses can be used to characterize majority and minority carrier traps respectively [5]. The effect of a pulse bias on filling and emptying process in P^+N junction diode is shown in Fig. 2.2. The pulse used is a majority carrier pulse. In subsequent sections, both capacitance and current transient signal expressions will be derived for a majority carrier pulse in a P^+N Jn.

2.2.2 Theory of Capacitance Transients:

The transition capacitance in a junction diode is given by $i = C_T \frac{dv}{dt}$. From Poisson's equation and its solution we get

$$V_j = \frac{qN_I W^2}{2\varepsilon} \qquad (2.14)$$

where W is the width of depletion region, N_I the concentration of ionized impurities in it, ε the permittivity within it and V_j the junction potential.

From eqn. (2.14) and $C_T = \frac{\varepsilon A}{W}$, one gets

$$C_T^2 = \frac{A^2 \varepsilon q N_I}{2V_j} \qquad (2.15)$$

For an acceptor level in a P^+N junction, $N_I = N_D - n_T$ and hence eqn. (2.15) becomes

$$C_T^2 = \frac{A^2 \varepsilon q}{2V_j} (N_D - n_T) \qquad (2.16)$$

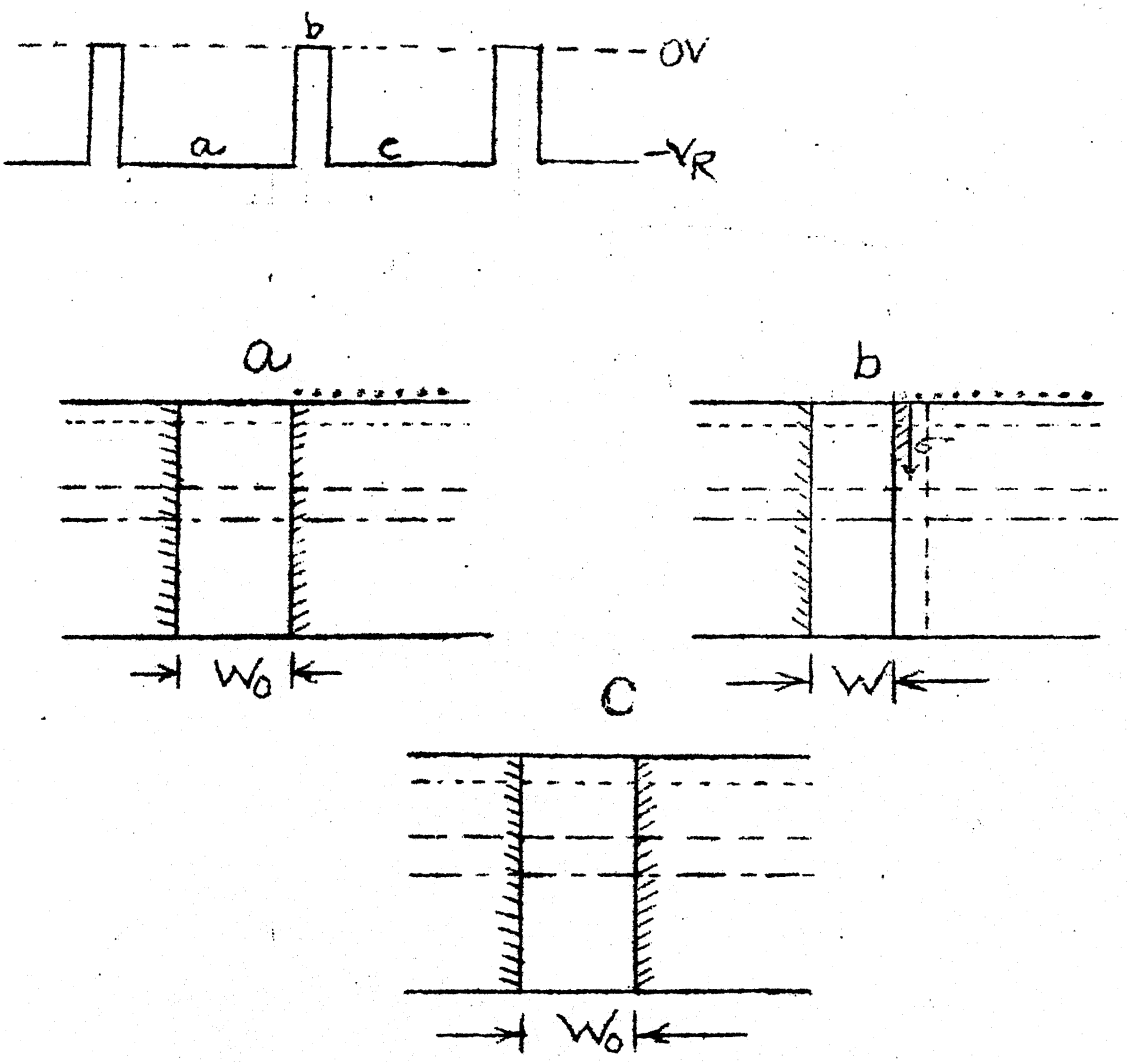

Fig. 2.2: 1) Majority carrier pulse (2)-(4): Energy band diagram showing depletion region (with shaded lines) as well a capture, emission and trap occupation during the three states a,b and c of the majority carrier pulse.

or

$$C_T = C_m \left[1 - \frac{\Delta C(t)}{C_m} \right] \qquad (2.17)$$

where,

$$C_m = \frac{A^2 \; q \; N_D}{2V_j}$$

and $$\frac{\Delta C(t)}{C_m} = \frac{n_T}{2N_D} \qquad (2.18)$$

Using eqn. (2.13) a and for acceptor level $e_n >> e_p$, we get for (2.18)

$$\frac{C(t)}{C_m} = \frac{n_T(o)}{2N_D} e^{-t/\tau_n}$$

$$= \frac{N_{TT}}{2N_D} e^{-t/\tau_n} \qquad (2.19)$$

Thus capacitance transient from a majority carrier pulse gives value of τ_n directly. Using eqn. (2.6), one can obtain values of activitation energy and capture cross-section. The initial value of transient has information regarding the trap concentration.

2.2.3 Theory of Current Transients:

The pulse sequence applied in this case, too, is as in Fig.2.2(1).As the voltage switches from O to $-V_R$, three components are obtained in the current transient signal.

1. A fast component in the form of a spike of very short duration is produced due to sweep out of majority carriers in the part of depletion region, which gets affected due to pulse bias sequence.

2. The slow current transient due to trap occupation has two forms. One consisting of conduction due to electrons and holes and other due to displacement currents, because of induced charge in $x < o$ and $x > w$ region, due to $\frac{dn_T}{dt}$. The components of slow transient are shown in Figure 2.3.

The conduction current due to electrons

$$i_{c_n} = A \int_o^w q \left(\frac{dn}{dt}\right)_T dx$$

$$= A\, q\, e_n n_T(t)\, w(t) \qquad (2.20)$$

where A and w are area and width of junction respectively and n=o while using eq. (2.8).

3. The displacement current is given by

$$i_d(t) = A \int_o^w q\left(\frac{dn_T}{dt}\right)(x/w)dx$$

$$= \frac{qwA}{2}\left(\frac{dn_T}{dt}\right) \qquad (2.21)$$

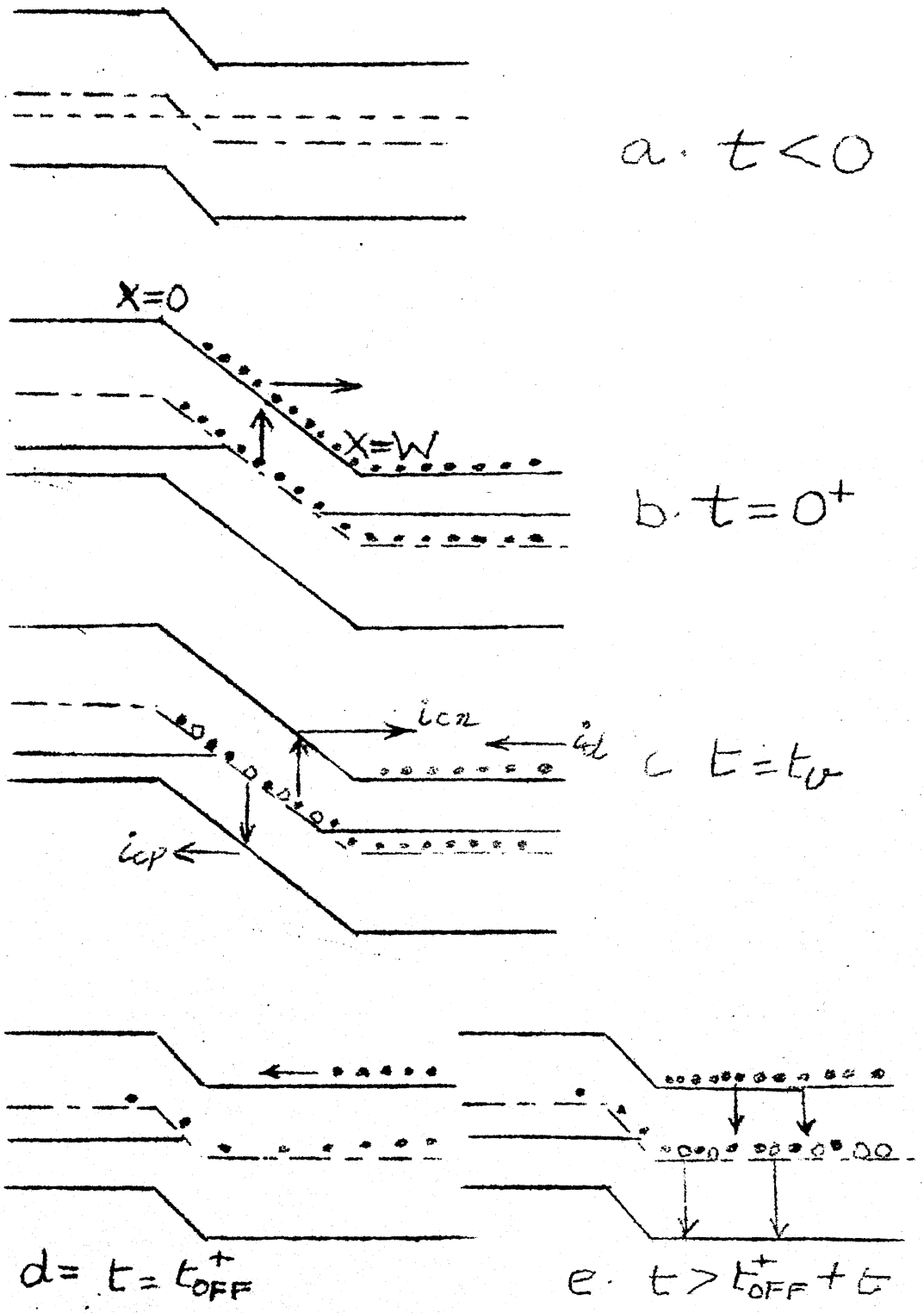

Fig. 2.3: Energy band diagram during the switching transients

Combining eqn. (2.20) and (2.21) and ignoring conduction current due to holes, which will be small in n-type semiconductor:

$$i = i_{c_n} + i_d = \frac{qWA}{2} (e_p p_T + e_n n_T) \qquad (2.22)$$

and for case of P^+N junction (2.22) becomes

$$i = \frac{qWA}{2} e_n n_T \qquad (2.23)$$

For an acceptor level (2.23) becomes

$$i = \frac{qWA}{2} e_n N_{TT} e^{-t/\tau_n} \qquad (2.24)$$

using the expression for W in (2.15) and (2.24) becomes

$$i = \frac{qW_\infty A e_n N_{TT}}{2} \left[1 - \frac{N_{TT}}{N_D} e^{-t/\tau_n} \right]^{-1/2} e^{-t/\tau_n} \qquad (2.25)$$

where,

$$W_\infty = \left[\frac{2\mathcal{E}V_j}{q N_D} \right]^{1/2}$$

If $N_{TT} << N_D$, (2.25) becomes:

$$i = \frac{qAe_n N_{TT}}{2} W_\infty e^{-t/\tau_n} \qquad (2.26)$$

Hence the current transient is exponential when $N_{TT} << N_D$, otherwise it is nonexponential.

The timing diagram for both current and capacitance transient in case of majority carrier pulse is shown in Fig. 2.4.

2.3 TECHNIQUES USED IN ANALYSIS OF TRANSIENTS:

This section briefly discusses the various techniques used to get trap data. They are essentially of two types called single shot methods and synchronous detection methods. In both the aim is to get Arrhenius plot.

2.3.1 Single Shot Methods:

They were historically the first methods to be used for analysis and are accurate but are very painstaking. Prime examples of this in our case are conventional isothermal capacitance transient study and isothermal current transient study [4]. Herein the time constants of transients are found and each point in Arrhenin's plot is obtained thereby.

2.3.2 Concept of DLTS:

Deep Level Transient spectroscopy is a synchronous detection method. It has been used very extensively in getting trap parameters. The major feature of this method is that it is fast, sensitive and spectroscopic in nature [5]. A wide variety of traps can be detected by observing

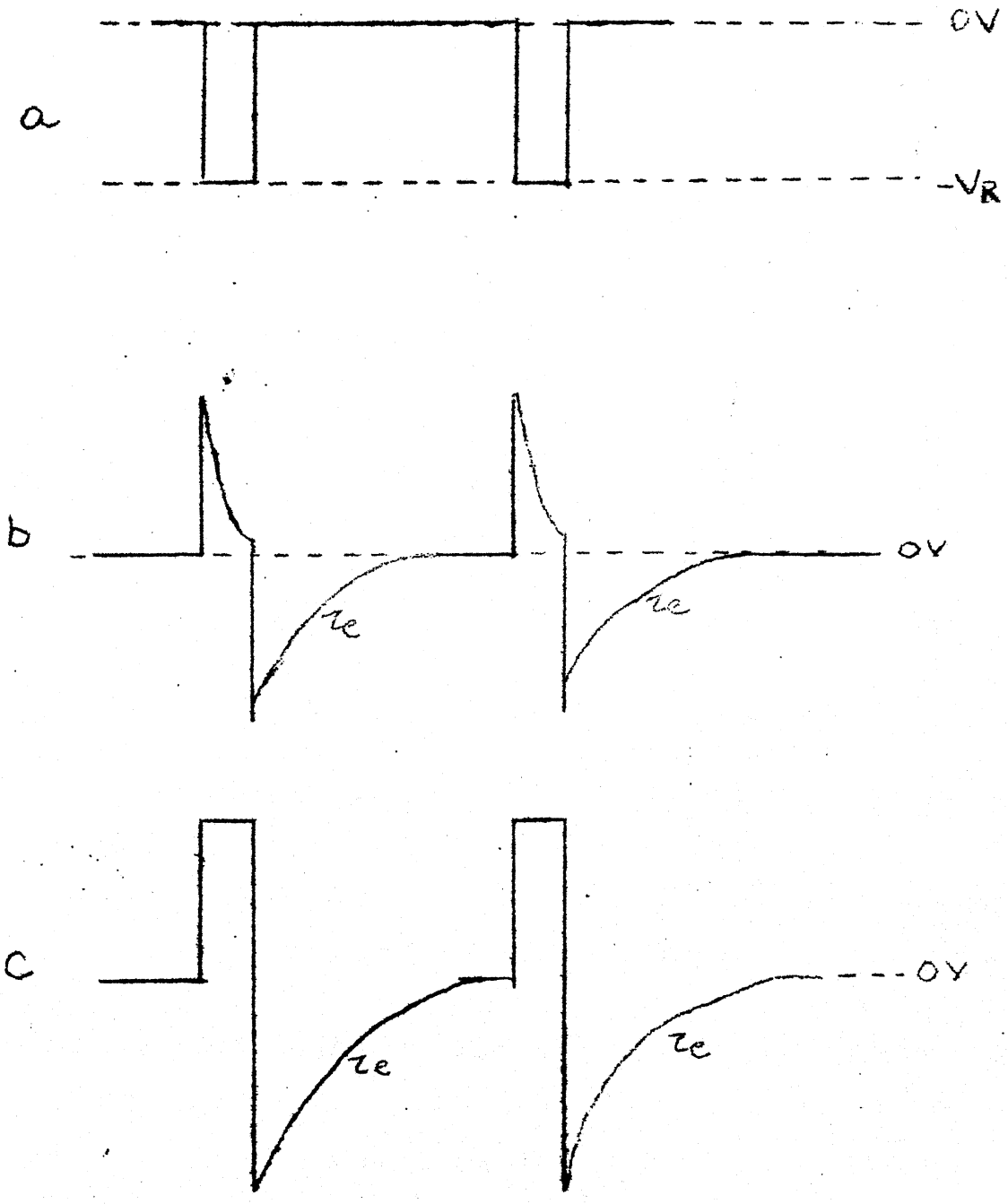

Fig. 2.4: Timing diagram of
b) current transients and c) capacitance transients corresponding to majority carrier pulse in (a).

the DLTS spectrum. The essential feature of DLTS is that one can set a rate window in a Box-car integrator as depicted in Fig. 2.5. The difference signal $C(t_1)-C(t_2)$ or $i(t_1)-i(t_2)$ is plotted as a function of temperature. The sign of the trap tells whether it is an electron or a hole trap and temperature corresponding to maximum gives one point on the Arrhenius plot. The value of e_n(or e_p) needed can be related to difference (t_1-t_2) through following:

Normalised DLTS signal is given by

$$= [C(t_1) - C(t_2)]/\Delta C(o)$$

where $C(o)$ is the capacitance change at $t = o$.

For exponential transients

$$S(t) = [\, e^{-t_1/\tau} - e^{-t_2/\tau} \,] \qquad (2.27)$$

where τ is the time constant of the transient.

Maximising eqn. (2.27) with respect to by differentiating and equating it to zero gives

$$\tau_{max} = (t_1-t_2)\,[\ln [t_1/t_2]] \qquad (2.28)$$

Thus one needs simply to scan the temperature and observe the DLTS spectra for each scan. The sign of peaks and position of peaks need to be observed and from this and

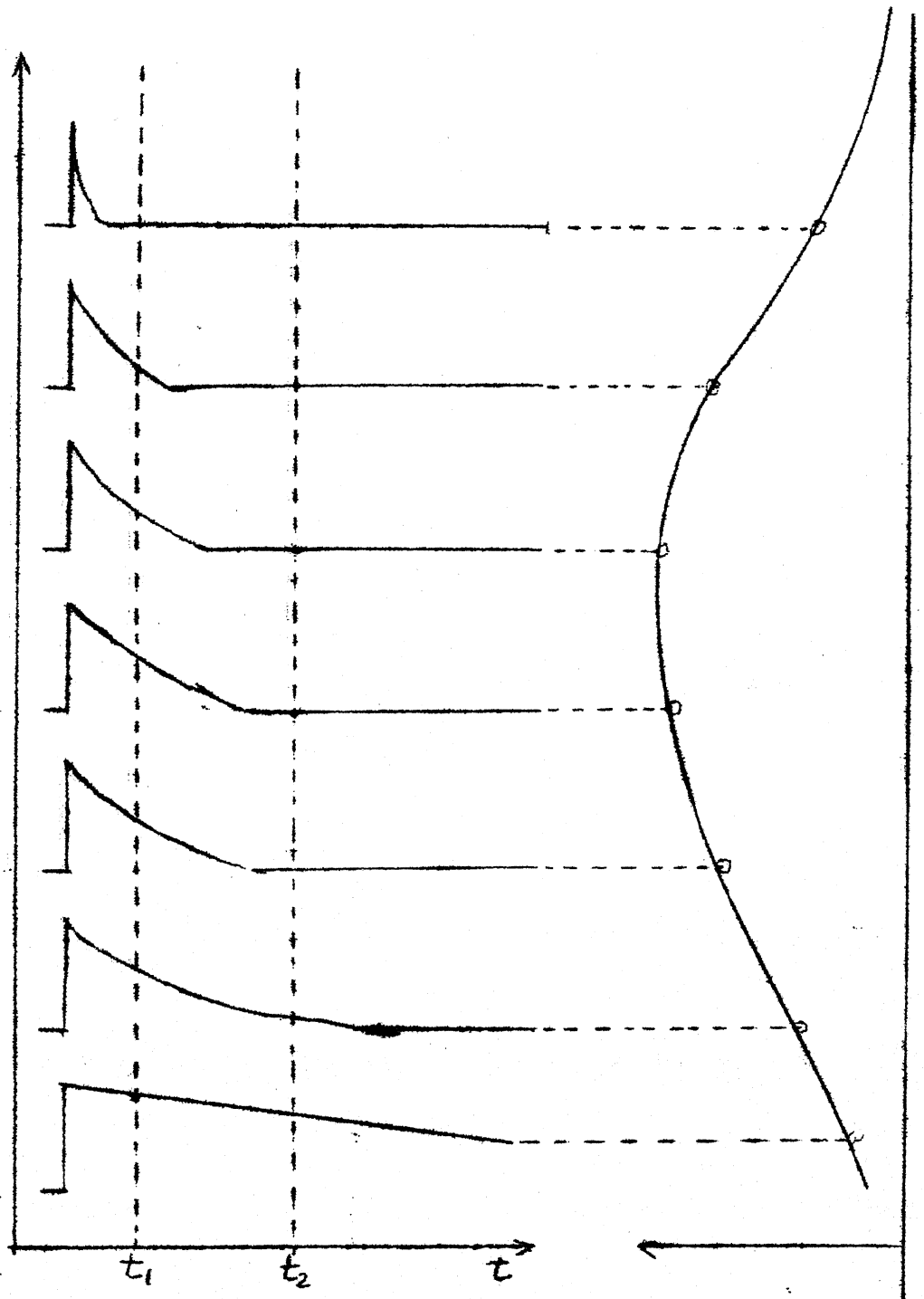

Fig. 2.5: Rate windowing concept.

values of t_1 and t_2 using eqn. (2.28), one can get an Arrhenins plot. Some remarks are in order:

1. This method is applicable to exponential transients only as evident from eqn. (2.27). Any non-adherence to this criterion will give wrong values for activation energy, capcture cross-section and related parameters [7]. It has been further found that choice of t_1 and t_2 can give widely different Arrheni s plots in such cases.

2. Even for a single exponential, the conventional DLTS uses inefficiently the data, it gets in each scan. Hence modifications have been suggested [8] where the rate windowing concept is done in software after recording all the transients in a single scan.

3. DLTS subtracts the offset due to leakage current or steady state capacitance and thus overcomes a serious problem affecting the single shot analyses.

4. Finally DLTS is at best a very good survey technique and can in no way supplant careful and accurate determination possible through single shot analysis.

CHAPTER 3

TRANSIENT DATA ANALYSIS

3.1 INTRODUCTION:

The isothermal relaxation data is characterized by two major factors:

a) That the transients sit on a steady state level ΔI_o or ΔC_o, leading to the form $Ae^{-\alpha t} + B$.

b) That in the presence of multiple traps, the data has multiexponential decay of the form $\sum_{i=1}^{n} A_i e^{-\alpha_i t}$.

At the outset, one might feel that determination of the values of A_i and α_i in the above is a trivial problem. However, it is not so [11]. Even for a single exponential case in (a) above to get an accurate and reliable value for A, α and B is a difficult exercise. In this chapter these aspects of the problems have been studied.

3.2 ANALYSIS FOR SINGLE EXPONENTIAL:

Initially the problem of determination of decay constant in single-exponential transient seems very easy. One can think of simply finding the ratio of the transient curve at two values and computing the decay constant. Or one could fit the logarithm of the transient curve to a

straight line using linear regression algorithm, thereby getting both A and α. However the offset B frustrates any such simple implementation. Hence the aim is to somehow remove this B and use the conventional methods thereafter or devise a suitable algorithm which takes B into account. The problem is further exacerbated by certain limitations of the signal analyser, detailed later on in the chapter. In any case, one has to be careful. Several methods have been suggested to remove this B accurately. Particularly in case of isothermal relaxation two ways were found to determine the value of B:

a) One uses the physical origin of this constant offset. In either current or capacitance transients, ΔI_o or ΔC_o emanate from the leakage current or steady state junction capacitance during the time of reverse bias in both minority carrier and majority carrier pulses. Hence for a given device, one can reverse bias it to the same conditions as that of pulses and obtain values of ΔI_o and ΔC_o. However the major problem in this lies in obtaining identical conditions repeatedly for each temperature. Hence it is not a very attractive method.

b) The other method to determine B, is to take average of a number of points on the tail of the transient and then subtract this average value from the whole curve.

However, scatter due to noise in the signal precludes dependence on only a few points. Hence one needs to take a large enough number of points on the tial portion so that randomness of noise cancels and helps in accurate determination of B. Such requirement, particularly, in case of low temperature slow transients is not readily possible.

One can then think of logical extension of the basic methods. One such extension is:

3.2.1 Ratio Method:

Herein we take three points on the transient and solve the resulting transcendental equation. Its brief description is as follows:

Three points on the transient curve $Ae^{-\alpha t} + B$ are:

$$y_1 = Ae^{-\alpha t_1} + B \qquad (3.1)$$

$$y_2 = Ae^{-\alpha t_2} + B \qquad (3.2)$$

$$y_3 = Ae^{-\alpha t_3} + B \qquad (3.3)$$

From eqns. (3.1), (3.2) and (3.3), we get

$$y_2 - y_1 = A(e^{-\alpha t_2} - e^{-\alpha t_1}) \qquad (3.4)$$

$$y_3 - y_2 = A(e^{-\alpha t_3} - e^{-\alpha t_2}) \qquad (3.5)$$

Using eqn. (3.4) and eqn. (3.5), one gets

$$\frac{y_2-y_1}{y_3-y_2} = \frac{e^{-\alpha t_2} - e^{-\alpha t_1}}{e^{-\alpha t_3} - e^{-\alpha t_2}} \qquad (3.6)$$

Values of y_1, y_2, y_3, t_1, t_2 and t_3 are known from the transient data and one has to solve this transcendental equation. Using Newton-Raphson method, one can solve this iteratively. Normally one should get a reliable and satisfactory result. However numerical snags come up, when evaluating it. This is because even slight variations in the values of t_1, t_2 or t_3 gives widely varying values of α_i's. Actually this is symptomatic of all problems dealing with exponentials. This method, therefore, demands very accurate measurements of t_1, t_2 and t_3. Table 3.1 emphasizes the above contention. An alternative method is, hence thought of:

3.3.2 Area Method:

Here transient with a positive d.c. shift is assumed, though for negative offsets too, the same procedure holds. A (current) transient from the relaxation process with a positive offset is shown in Fig. 3.1.

The three equations in this case are:

$$X_1 = A + B \qquad (3.7)$$

Table 3.1: Results from ratio method analysis

t_0 in μs	t_1 in μs	t_2 in μs	t_3 in μs	A	α	B
0	0	0	0	0.285603	13610.6	0.226716
+2β	X	X	X	0.267275	13621.6	0.22678
+2β	X	X	X	0.233989	13631.7	0.226838
-2β	X	X	X	0.305109	13592.2	0.226608
-6β	X	X	X	0.348874	13633.9	0.226851
0	+2β	0	0	0.281506	12557.3	0.220042
0	+4β	0	0	0.279169	10867.5	0.206545
0	+6β	0	0	0.312894	6533.76	0.139164
0	-2β	0	0	0.287909	14063	0.229265
0	-4β	0	0	0.295239	15257	0.235239
0	-6β	0	0	0.292871	14884	0.233479
0	-10β	0	0	0.300032	15863	0.237912
0	0	+2β	0	0.291945	16529.6	0.242591
0	0	+4β	0	0.290297	16061.2	0.240467
0	0	+6β	0	0.287189	14965	0.234946
0	0	+10β	0	0.292163	10658.4	0.200881
0	0	-4β	0	0.297631	17829.1	0.24783
0	0	-6β	0	0.295431	17367.7	0.246071
0	0	0	+4β	0.285849	13564	0.226259
0	0	0	+6β	0.290505	12782.7	0.218111
0	0	0	+10β	0.28221	14338.3	0.233456
0	0	0	-4β	0.291403	126505	0.216632
0	0	0	-6β	0.293571	12349.9	0.213153
0	0	0	-15β	0.349857	8266.78	0.1405
0	+2β	+4β	+10β	0.287851	15939.9	0.240383
0	-10β	-15β	+10β	0.299729	17945.7	0.246896
+3β	+5β	-7β	+2+	0.259482	16174.4	0.239715
-2β	-5β	+4β	+9β	0.319644	16026.8	0.238732

t_1 = 43.9451 μs, t_2=68.359 μs, t_3=117.187 μs, t_0 = 0

β = 2.4414 μs, X = Corresponding change, t_1, t_2 etc - changes in t_1, t_2 etc.

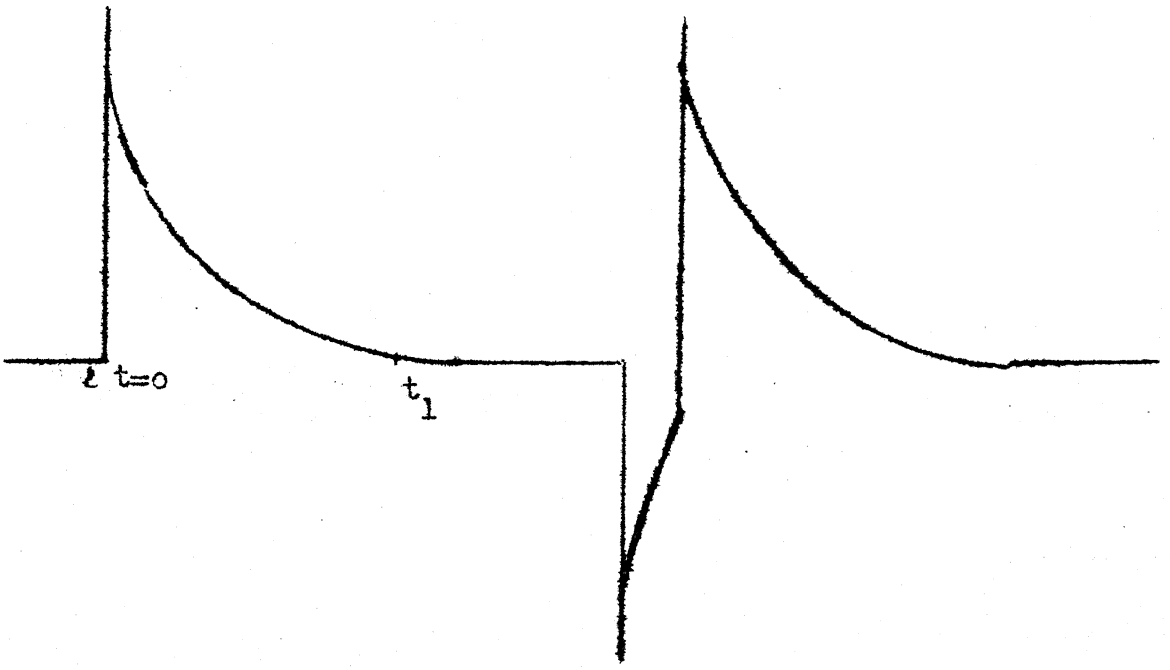

Fig. 3.1: A typical (current) transient.

$$X_2 = Ae^{-\alpha t_1} + B \qquad (3.8)$$

and

$$K = \int_0^{t_1} (Ae^{-\alpha t_1} + B)\, dt \qquad (3.9)$$

eqn. (3.9) on evaluation, gives

$$K\alpha = A[1-e^{-\alpha t_1}] + B\alpha t_1 \qquad (3.10)$$

Using $B = X_1 - A$ from eqn . (3.7) in eqn. (3.8) we get for A,

$$A = \frac{X_1 - X_2}{(1-e^{-\alpha t_1})} \qquad (3.11)$$

Substituting eqn. (3.11) in eqn. (3.10), we get:

$$(X_1-X_2)[1-\alpha t_1-e^{-\alpha t}] = (1-e^{-\alpha t_1})\,(K-X_1 t_1)\alpha \qquad (3.12)$$

The above transcendental equation can be solved by observing the zero cross-over, for monotonically increasing α.

The values of [illegible] obtained from this method have been found to be accurate and less susceptible to initial data variations than the Ratio method. Table 3.2 illustrates the above point. It further shows that the variation in α value with different choices of t_o ($t=o$) is not acceptable. Unfortunately an accurate determination of t_o is not easily possible for current transients. This is precisely due to two factors:

Table 3.2

Results from Area Method

t_0	t_1	α	B
0	0	12825	0.216796
$+2\beta$	0	9775	0.216796
$+6\beta$	0	9675	0.216796
-2β	0	13825	0.216796
-4β	0	9525	0.216796
0	$+2\beta$	13550	0.217285
0	-2β	14550	0.217285
0	-4β	14225	0.218261
0	-6β	16025	0.219726
$+2\beta$	-2β	10100	0.219726
-3β	-4β	10000	0.218261
$-\beta$	$+\beta$	9500	0.217285

$t_0 = 0$, $t_1 = 2.13378$ ms, $\beta = 2.4414$ μs

t_0, t_1 - changes in t_0 and t_1 respectively.

a) 100 KHz bandwidth of the signal analyser and hence existence of reasonably strong Gibb's effect.

b) A large current component due t_o sweep-out of majority carriers in the sample, saturates the current transient measurement set-up.

The cumulative effect of both is that accurate t_o determination is not possible. However the redeeming feature of the area method, as from Table 3.2, is that the variations in B, due to fluctuations in choice of t_o instant are very small. Therefore our analysis for single exponential transients with offset, starts with Area method, where from the value of B is determined. This B is subtracted from the total curve and conventional methods are applied to get the values of A and α accurately.

The above analysis proceeds on the assumption that a single exponential decay is present. What if it is not so, as it is in the case of multiple traps where we may force unknowingly a multiexponential of the form $\sum_{i=1}^{n} A_i e^{-\alpha_i t}$ to a single exponential. According to Lanczos [11], satisfaction of equivalence of the measured results to the computed ones using either one or more decay constants is no indicator of the actual values. For example the data in Table 3.3 for a double exponential signal can be, within

Table 3.3: Illustration of numerical equivalence of two different exponential expressions.

t in microseconds	Actual double exponential $1e^{-5000t}+2e^{-10000t}$	Least square single exponential $2.98375e^{-8056.71t}$
0	2.99988	2.98372
2.4414	2.93957	2.92562
4.8828	2.88049	2.86863
7.32418	2.82275	2.81276
9.76558	2.76623	2.75797
12.2069	2.71094	2.70426
17.0897	2.60388	2.59994
21.9725	2.50134	2.49964
24.4139	2.45178	2.45096
26.8553	2.4032	2.40322
34.1795	2.26379	2.26551
39.0623	2.17579	2.17811
43.9451	2.09155	2.09412
51.2693	1.97168	1.97416
56.152	1.896	1.89804
63.4762	1.78845	1.78937
70.8004	1.68701	1.68697
80.5659	1.56201	1.55961
85.4428	1.5033	1.49966
90.3315	1.44702	1.44109
95.2144	1.39307	1.3855
100.097	1.34131	1.33205

Least mean square error for 300 points = $.151819 \times 10^{-2}$

the accuracy of measurements, fitted to a single exponential. Comparing the two data lists one finds that error indeed is very small. In order to be more confident in case of single exponential analysis as well as to ascertain the existence of multiple traps, it is mandatory to know values of n, A_i and α_i in $\sum_{i=1}^{n} A_i e^{-} i^{t}$. This is dealt in next section.

3.3 ANALYSIS FOR MULTIEXPONENTIAL SIGNALS:

Several methods are known for this important analysis According to Lanczos [11], it is not the limitation of the methods of analysis, which gives us unsatisfactory results but that the accuracy of initial data is not good enough to take care of extreme sensitivity of exponentials to scatter in initial data. Hence a method due to Gardner et.al. [12] is described. In this method the end result is in the form of peaks corresponding to each of the exponents in the multiexponential signal. This method is subdivided into three main subsections viz. theory, implementation & results and application to relaxation data.

3.3.1 Theory:

We are given the function $f(t) = \sum_{i=1}^{n} A_i e^{-\alpha_i t}$ and we wish to determine n, A and α_i. The above Dirichlet series is converted to Stieltjes integral:

$$f(t) = \sum_{i=1}^{n} A_i e^{-\alpha_i t} = \int_0^{\infty} e^{-\alpha t}\, dh(\alpha) \qquad (3.13)$$

where $h(\alpha)$ is a sum of step functions. Eqn. (3.13) can be expressed in terms of Delta functions as:

$$f(t) = \int_0^{\infty} e^{-\alpha t}\, g(\alpha)\, d\alpha \qquad (3.14)$$

The quantity $g(\alpha)$ contains information about the various α_i values. The aim is hence to solve for $g(\alpha)$. The solution of this integral equation is done by transforming the variables α and t as $\alpha = e^{-y}$ and $t = e^{x}$.

Then eqn. (3.14) becomes

$$f(e^{x}) = \int_{-\infty}^{\infty} \exp[e^{-(x-y)}]\, g[e^{-y}]\, e^{-y} dy \qquad (3.15)$$

comparing eqn. (3.14) and (3.15), one finds

$$g(\alpha)d\alpha = \alpha g(e^{-y})dy$$

or

$$\left(\frac{g(\alpha)}{\alpha}\right)d\alpha = g(e^{-y})dy \qquad (3.16)$$

Hence a plot of $g(e^{-y})$ with respect to y is equivalent to plot of $g(\alpha)$ with respect to α. Therefore we need to find ways to get $g(e^{-y})$ from eqn. (3.17). We multiply eqn. (3.15) by $t=e^{x}$, then eqn. (3.15) becomes:

$$e^{x} f(e^{x}) = \int_{-\infty}^{\infty} \exp[-e^{x-y}]\ e^{x-y}\ g(e^{-y})dy \qquad (3.18)$$

We define Fourier transform $F(\mu)$ as

$$F(\mu) = \frac{1}{\sqrt{2\pi}} \int_{-\infty}^{\infty} e^{x} f(e^{x}) e^{i\mu x}\ dx \qquad (3.19)$$

Hence eqn. (3.18) becomes using eqn. (3.19),

$$F(\mu) = \frac{1}{\sqrt{2\pi}} \int_{-\infty}^{\infty} \int_{-\infty}^{\infty} \exp[-e^{x-y}]\ e^{x-y} g(e^{-y})dy\ \exp(i\mu x)dx \qquad (3.20)$$

Putting $s = x-y$ and $x = s+y$ in eqn. (3.20) one gets:

$$F(\mu) = \frac{1}{\sqrt{2\pi}} \int_{-\infty}^{\infty} \int_{-\infty}^{\infty} \exp[-e^{s}]\ e^{s}\ g(e^{-y})dy \exp(i\mu(s+y))ds \qquad (3.21)$$

or eqn. (3.21) becomes

$$F(\mu) = \frac{1}{\sqrt{2\pi}} \int_{-\infty}^{\infty} g(e^{-y})\ \exp(i\mu y\ dy \int_{-\infty}^{\infty} \exp(-e^{s})e^{s} \exp(i\mu s)ds \qquad (3.22)$$

In eqn. (3.22), one finds that first integral can be called Fourier Transform $G(\mu)$ of $g(e^{-y})$, while the second integral needs to be found separately. However the second integral

can be related to Euler integral of complex Gamma function, which is given by:

$$\Gamma(z) = \int_{-\infty}^{\infty} e^{-t}\, t^{z-1} \quad \text{for} \quad \quad > o \tag{3.23}$$

Substituting $t = e^{s}$ in eqn. (3.23) one gets

$$\Gamma(z) = \int_{-\infty}^{\infty} \exp(-e^{s})\, e^{s(z-1)}\, e^{s}\, ds \tag{3.24}$$

If $z = 1+i\mu$, then

$$\Gamma(1+i\mu) = \int_{-\infty}^{\infty} \exp(-e^{s})\, e^{i\mu s}\, e^{s}\, ds \tag{3.25}$$

This is what exactly is the second integral in eqn. (3.22). Fortunately values of Gamma function are available in tabulated form. Defining $K(\mu)$ as

$$K(\mu) = \frac{1}{\sqrt{2\pi}}\, \Gamma(1+i\mu)$$

one gets from eqn. (3.22),

$$F(\mu) = K(\mu) \cdot G(\mu)$$

or

$$G(\mu) = \frac{F(\mu)}{K(\mu)} \tag{3.26}$$

If one takes the inverse Fourier transform of eqn. (3.26), then one gets

$$g(e^{-y}) = \int_{-\infty}^{\infty} G(\mu)\ e^{-i\mu y}\ d\mu \qquad (3.27)$$

Hence a plot of $g(e^{-y})$ with respect to y will give the value of exponents as peaks, the amplitudes of which are proportional to N_i/α_i.

3.3.3 Implementation and Results:

The above algorithm is implemented using BASIC program on the signal analyser (IWATSU model SM2100B). The integrations are done by Simpson's method. The listing of the program is given in Appendix II. To prove the method, both analytical and experimental data were taken. Figs. 3.2 to 3.5 illustrate the results of the analysis. The analysis is in the form of a plot of $g(\alpha)$ as a function of α. However such a plot cannot be directly obtained in the signal analyser, primarily because of the fact that a given function can be displayed only at discrete instants of time. The functional values at each of these instants are stored in the form of an array in the memory. These array locations are accessible through software. The above fact is exploited by storing α and $g(\alpha)$ values simultaneously in two different arrays. And when the two arrays are displayed, the values read by the cursor at each instant give the values of $g(\alpha)$ and α.

To appreciate the multiexponential analysis, four examples in Figs. 3.2 to 3.5 are used to illustrate its various details:

1. All the plots in each figure show a spectra like behaviour. This is so because of finite cut offs for x and μ variables in eqn. (3.18) and eqn. (3.27). For instance eqn. (3.18) with finite cut offs for x and μ is given by:

$$F(\mu) = \frac{1}{\sqrt{2\pi}} \int_{-x_o}^{+x_o} . e^x f(e^x) \exp(i\mu x) dx + E[x_o, \mu] \qquad (3.28)$$

The extra term above is an indicator of the error due to cut offs in x and μ. This error manifests itself in eqn. (3.26) where $F(\mu)$ is divided by $K(\mu)$. As the values of μ are increased, the $K(\mu)$ values decrease very rapidly and a small error $E(x_o, \mu)$ in $F(\mu)$ gets amplified to large error peak. This can be seen in Figs. 3.2 to 3.4 where as μ is increased from $\mu=3$ to $\mu=5$ and then to $\mu=7$, the number of peaks increases. In Fig. 3.5, the same thing is observed for $\mu=2$, $\mu=4$ and $\mu=6$.

2. The existence of error peaks in these can lead to loss of peaks, corresponding to actual α_i values. However the redeeming feature of this method is that as one varies values of μ, the error peaks shift their position while real peaks do not. This is shown in each of the figures and for each of the μ's by placing the cursor at the peak or peaks, which move very little.

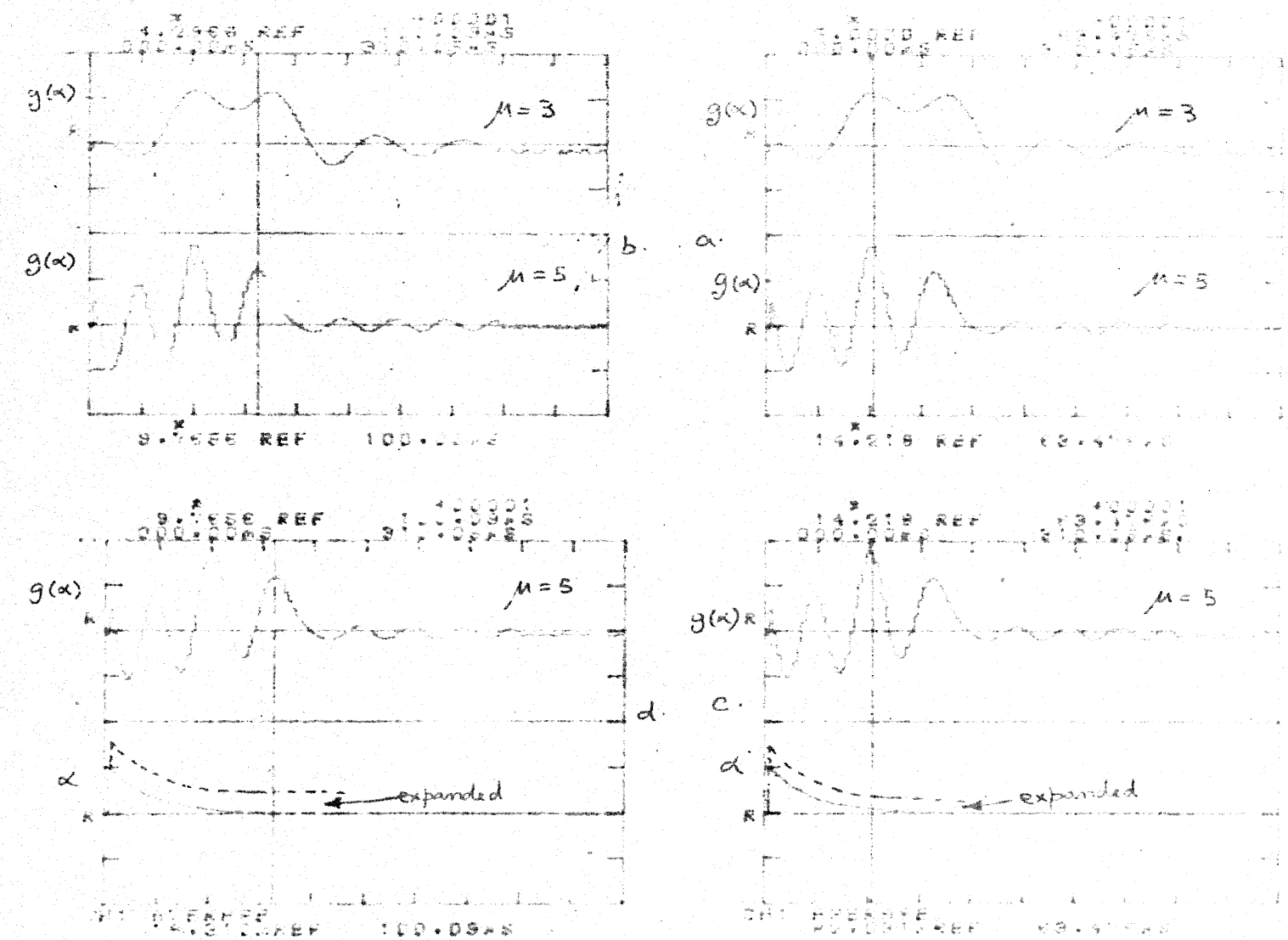

Fig. 3.3: Multiexponential analysis on analytically generated double exponential $1e^{-.016t} + 5\,e^{-.02t}$ values found: .01[illegible] and .0[illegible].

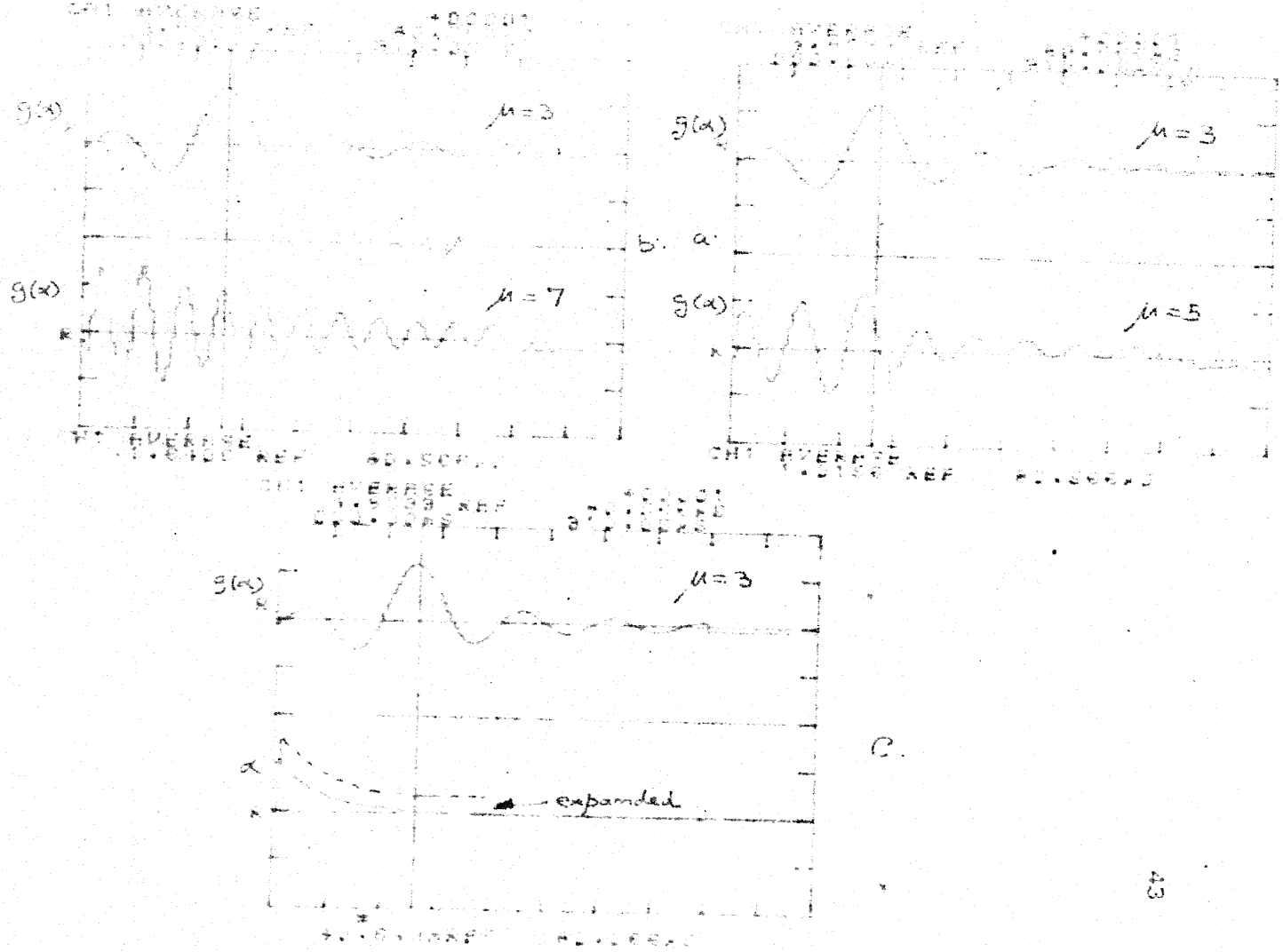

Fig. 3.4: Multiexponential analysis on experimentally obtained $1.0\ e^{-4000t}$ scaling factor = 100000 and a value found: 4004.9

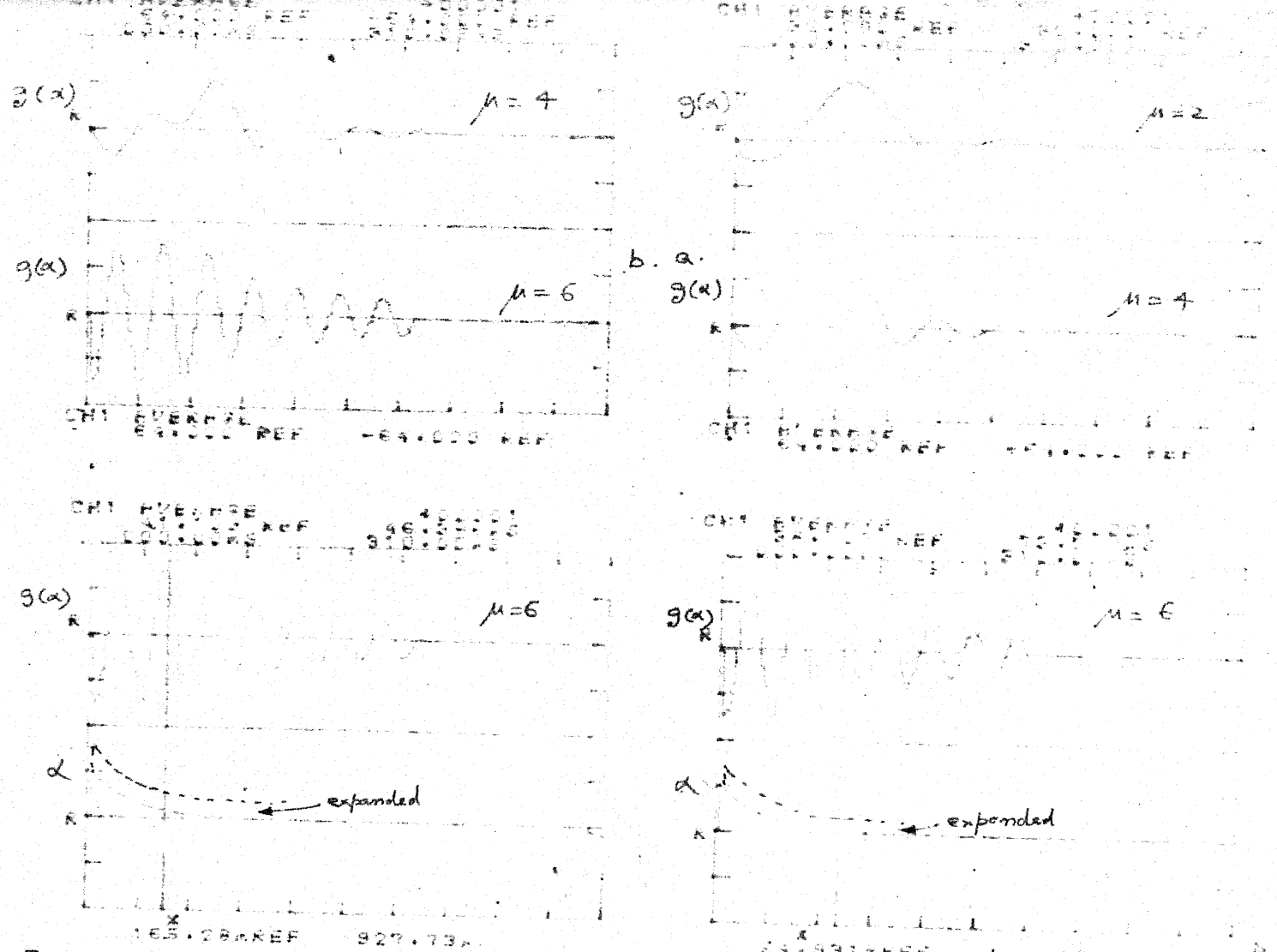

Fig. 3.5 Multiexponential analysis on experimentally obtained $1e^{-500ct} + 2e^{-100ct}$
Scaling factor: 100000, Values found for a_i's: 5493 & 16528

3. The resolution of each actual peak is maximum at higher μ's and hence accurate μ_i's can be known by increasing μ's gradually so that these are properly distinguished at lower μ's when error peaks are smallest and accurately known at higher μ's, where their resolution is maximum.

4. The variation in α in all figures 3.2 to 3.5 is from 0 to 1. Hence all decay constants need to be scaled in time so that α falls between 0 and 1. For instance in Fig. 3.4 an exponential of the form $100e^{-4000t}$ is used. For decay constant to fall between 0 and 1, it is scaled in time as $100e^{-.04x(100000t)}$. The result of the analysis then would give the peak of $g(\alpha)$ at $\alpha = .04$. The value as read from Fig. 3.4(c) shows this α value as .040649. Similarly scaling is done in Fig. 3.5. In both the figures hence the scaling factor used is 100000. As the exponentials of Fig. 3.2 and 3.3 have exponents less than one, therefore no scaling is needed in these cases.

5. For the case where more than one exponent is present, A_i should increase as α_i increases. For our illustration, the two double exponentials $1e^{-.016t} + 5e^{-0.8t}$ and $1e^{-5000t} + 2e^{-100000t}$ satisfy this condition.

6. Another precaution which needs to be taken is that the given exponential function should be properly sampled. If

the whole exponential information is not available as input to the algorithm, error is found in the determined α_i values. Fig. 3.6 shows how this particular effect in case of two different cut offs on the exponential gives a different α value. For the transient $100e^{-4000t}$, the values of $e^x f(e^x)$ are plotted in (a) and (b). The values along the abscissa are proportional to x values. In 3.6(a) the sampling is done till the exponential has totally decayed and in 3.6(b), the data obtained is only upto an earlier time instant, where the transient has not decayed completely. The results of the analysis show that for the case in 3.6(a), the peak occurs at 4064.9. This is seen in Fig. 3.6(c) while Fig. 3.6(d) shows α value as 5493.1 for abrupt cut off case.

7. Finally all the values found by multiexponential analysis in Figs. 3.2 to 3.5 are compared with the actual values. In Fig. 3.2, for analytical function $100e^{-.02t}$ the analysis is done at $\mu=3$, $\mu=5$ and $\mu=7$. Only one peak is seen to move very little along the abscissa. This peak is identified by the cursor and its value is read in (c) as .020141.

Fig. 3.3 analyses double analytic exponential $1e^{-.016t} + 5e^{-.08t}$. The μ value is varied from $\mu=3$ to $\mu=5$ to $\mu=7$. There are two peaks found to move very little and they are read in (c) and (d) as .018 and .082 respectively.

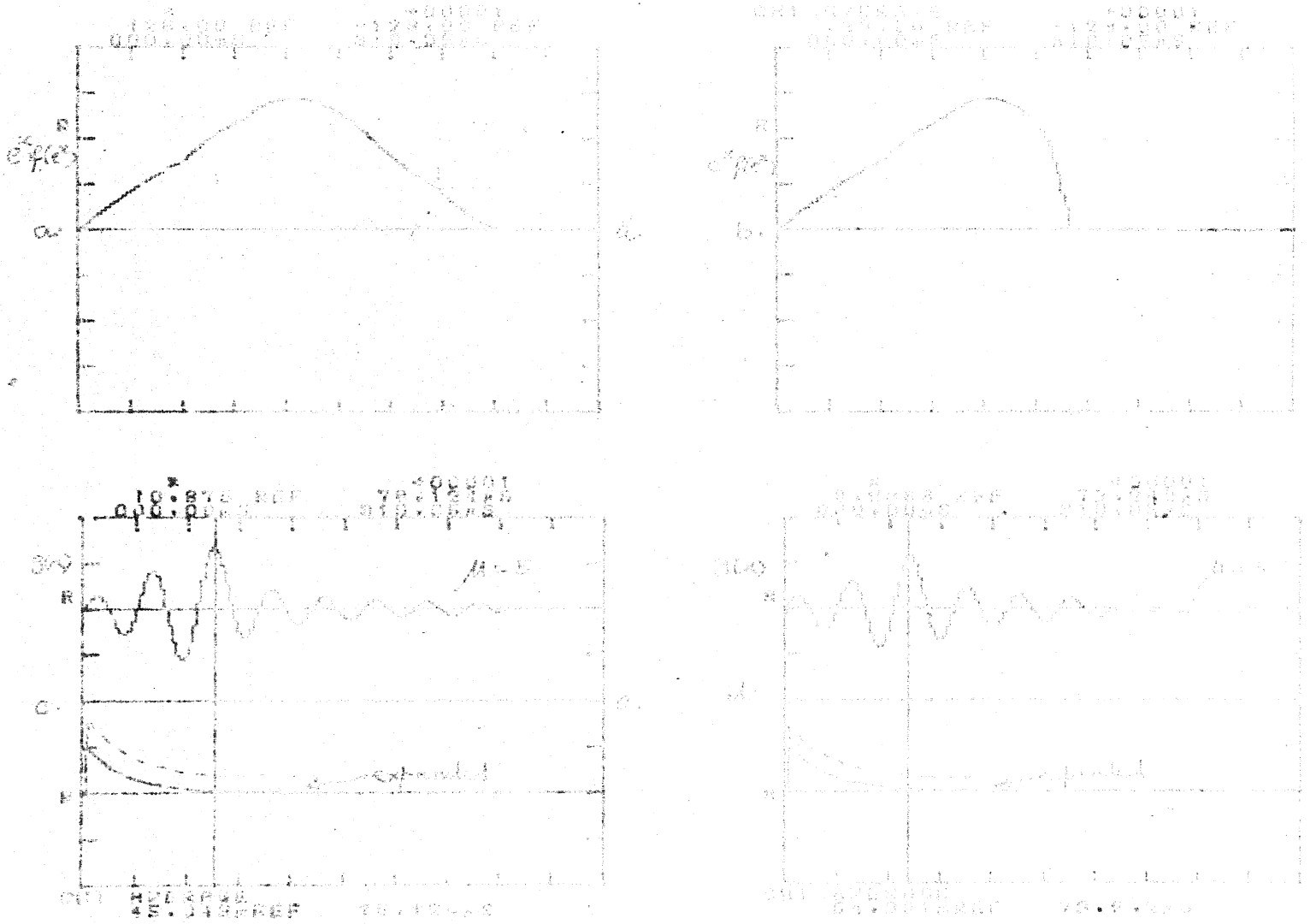

Fig. 3.6: Effect of cutoff in X in eq. (3.10) for [illegible] exponential [illegible]
(a),(c) total decay, (b),(d) [illegible]
for (a) [illegible] for (b)

In Fig. 3.4 experimentally obtained single exponential is analysed at $\mu=3$, $\mu=5$ and $\mu=7$. One peak as identified by cursor is shown to be almost stationary. The value of α at this peak is read in (c) as .040642. As the scaling factor of 100000 was used, the actual α value is 4064.2.

Lastly the double exponent $1e^{-5000t}$ and $2e^{-1000t}$ in Fig. 3.5 is chosen particularly since it was found using conventional methods that this was numerically equivalent to its least square fitted expression $2.98375\ e^{-8056.71t}$ as shown in Table 3.3. Now as the multiexponential analysis is done on it, the two exponents show themselves clearly as μ is varied from 2 to 6 as shown in Fig. 3.5(a) and (b) respectively. At $\mu=2$ there is seen a broad peak, which breaks into two as μ is increased to 4 and then to 6. The values of α_i's at these peak points are read in Fig. 3.5(c) and (d) as .054931 and 1.6528. Using the fact that scaling factor of 100000 was used, the actual α_i values are 5493 and 16528.

Thus it is seen that multiexponential analysis is very convenient to detect multiexponents since the number and values of components fall out of the analysis. The following subsections discusses its application to relaxation data.

3.3.4 Application to Relaxation Data:

Application to particular case of isothermal relaxation is considered here. The following points can be made.

1. This method is used to ascertain the number of components in the transient and get their approximate values.

2. Because of the limitation listed in (6) in Section 3.3.3, the results from an unknown sample need to be considered carefully.

3. μ values need to be varied from the lowest possible to the largest possible values so that the true peaks are unambiguously distinguished.

4. Major problems faced when implementing the algorithm on the signal analyser are its long execution time and limited accuracy. Both limitations contribute to the determination of only approximate values, taken over relatively long times. Needless to say given a faster and more accurate machine, it is possible to get fairly accurate spectra.

3.4 ANALYSIS FOR DLTS:

DLTS, as explained in Chapter 2, is an elegant procedure for characterizing deep levels, even in the presence of multiple traps, which have reasonably apart activation energies. It has advantages over the above

analysis procedures, since it is spectroscopic in nature. At the same time it retains the essential features of space-charge relaxation methods. The conventional DLTS, as mentioned in Chapter 2, uses inefficiently the data and requires a double Box-car integrator. For each point in Arrhenius plot, a separate thermal scan is needed. The time and effort needed for this are prohibitive for very large temperature variations. This disadvantage is overcome by separating the acquisition of signal from its analysis [8]. In this modified procedure, the isothermal capacitance and current are acquired and stored in memory of signal analyser. Corresponding to setting of rate window in Box-car integrator, a program is written, wherein variation of a single variable changes the rate window. A DLTS spectrum is thus obtained. However one should be careful in interpreting this data, since now temperature is held constant and not varied continuously.

CHAPTER 4

MEASUREMENT SYSTEM FOR DATA ACQUISITION

4.1 INTRODUCTION:

This chapter deals with the measurement aspects of capacitance and current transients. Both the signals have very low amplitude and hence are very noise prone. The capacitance measurement, particularly, has to be done at 500 KHz or above, since in order to monitor space charge capacitance, the monitoring signal should not disturb the transition capacitance. Section 4.2 deals with the measurement system used for data acquisition. Section 4.3 and 4.4 discuss, in particular, the design of capacitance and current measurement modules.

4.2 MEASUREMENT SYSTEM FOR DATA ACQUISITION:

The measurement system can be divided into four blocks, as shown in Fig. 4.1. A brief discussion is given for each block.

1. Cryostat:

This essentially contains a Liquid Nitrogen dewar and a sample holder to place the sample at various depths in the cryocan . The temperature variation can be done

84237

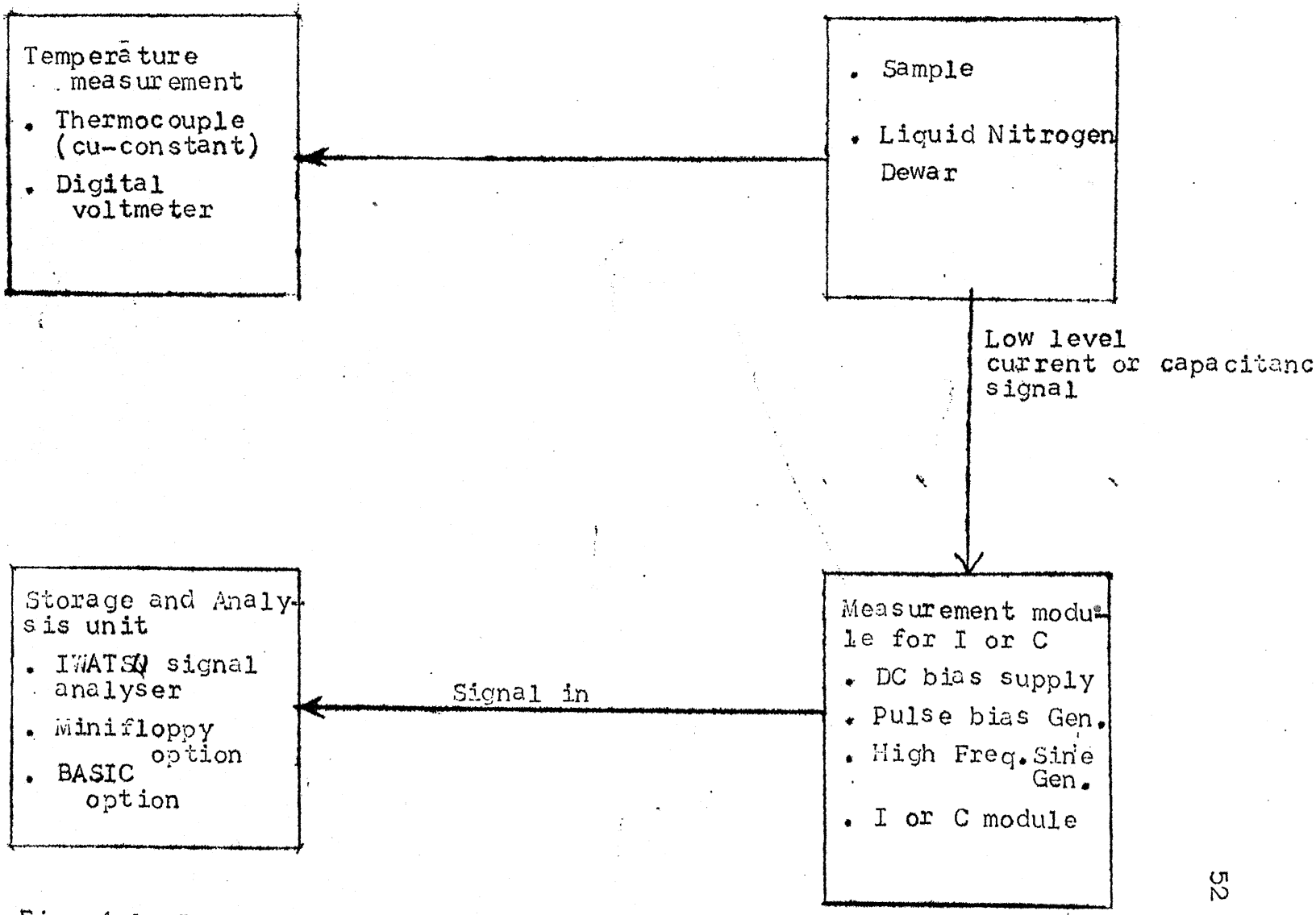

Fig. 4.1: Block diagram of measurement system for data acquisition.

exploiting the temperature gradient within the dewar. The temperatures above room temperatures can be obtained with the help of a soldering iron.

2. Temperature Measurement Block:

Temperature measurement is done with the help of a fine quality copper.- Constantan thermocouple. The thermocouple junction temperature is monitored directly with the help of a Digital multimeter (Keithley model 191). Room temperature correction is done after a mandatory warm up time of an hour or so. This is done by nulling this initial reading on the multimeter itself. An error of 2 to 3°C can result in absence of this correction.

3. Signal Acquisition Block:

The acquisition block consists of following accessories, each of which is briefly described.

a) D.C. bias supply: This is needed in case of minority carrier pulse when the sample needs to be slightly forward biased. It is normally superimposed on the pulse bias.

b) Pulse bias supply: This is used to obtain the majority and minority carrier pulses. Here the pulse should be negative going from 0 V to -10 V. The pulse generator

used should have pulse rise and fall times of the orders of microseconds. In this case, Yamuna Pulse Generator has been used.

c) High frequency sinewave Generator: This is particularly used in case of capacitance transient measurements. The exact need for it is explained in the design of capacitance measurement module. The model used is GR-1210C.

d) Capacitance measurement module: This is used for getting both majority carrier and minority carrier trap transients. High frequency (500 KHz or more) sinewave is used to monitor the capacitance changes in the space charge region. Its design is explained later on in Sec.4.3.

e) Current measurement module: It is also used to get transients from majority and minority carrier traps. Its design details, too, are explained later on in Section 4.4.

4. Recording and analysis block:

These functions are performed by IWATSU signal analyser (model SM-2100B). The options necessary for our applications are:

a) Averaging: It is needed to improve the S/N ratio of very noisy capacitance and current transients from

the sample diode. Summation averaging is used in this case.

b) Basic option: This option is used to obtain the various analys s programs described in chapter three.

c) Minifloppy option: This serves as our secondary storage unit for the current and capacitance transients. This helps in separating the acquisition from analysis, a desirable characteristic for DLTS.

4.3 DESIGN OF CAPACITANCE TRANSIENT MEASUREMENT MODULE:

The aim of this module is to measure the capacitance change in the transition region of the sample, during the relaxation process. At the outset, one realizes that the method used to measure capacitance should not disturb the charge condition in the depletion region. Hence the monitoring signal should be both small in magnitude as well as should be of high frequency such that charge change should be slower than it. Here this transient is measured using principle of phase-sensitive detection.

4.3.1 Theory of Phase Sensitive Detection:

The principle of phase sensitive detection can be explained using Fig. 4.2.

Here there are two channels one is the reference channel and other is the channel through system under test.

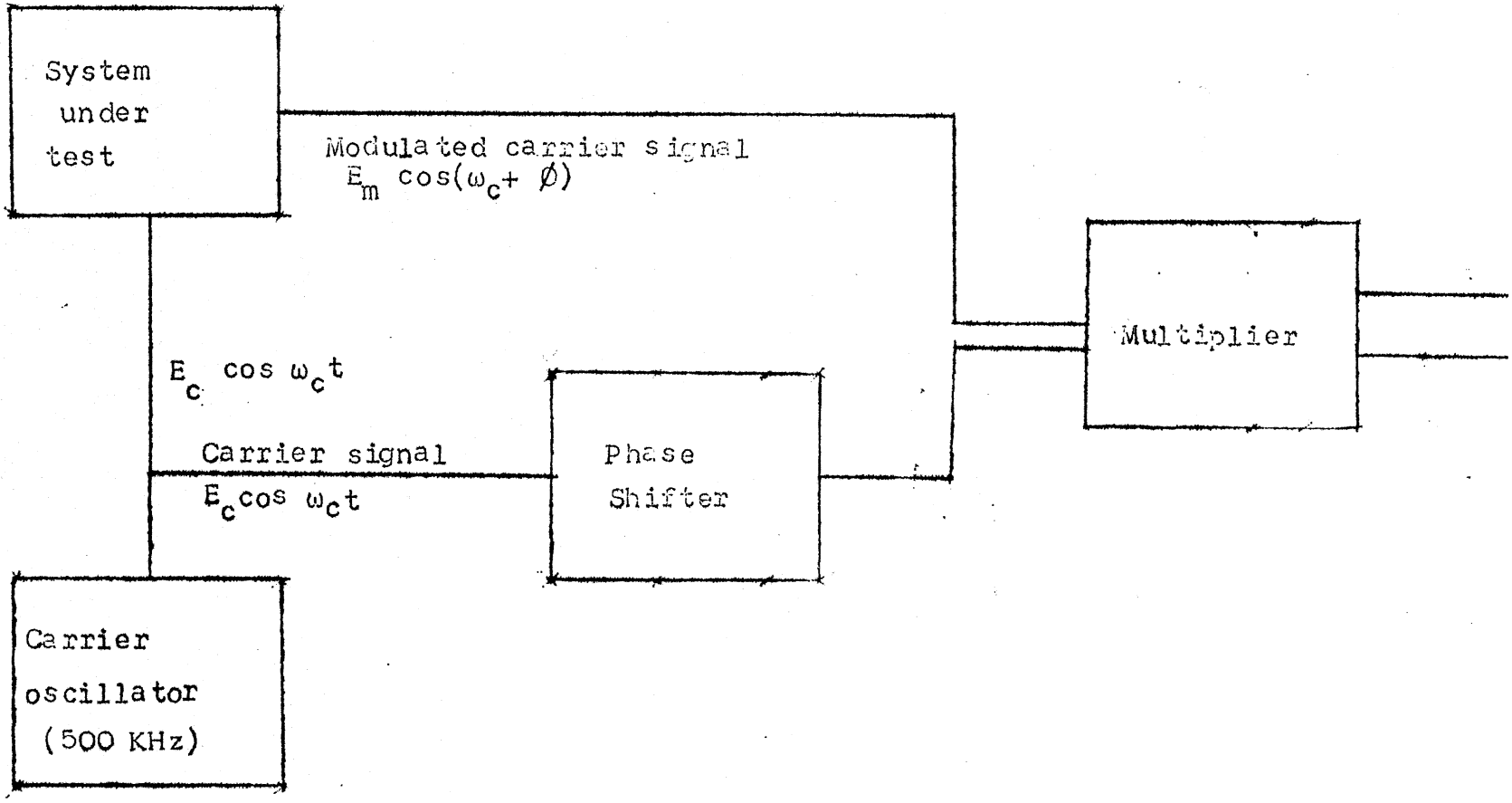

Fig. 4.2: Block diagram of a phase sensitive detector

Both the channels are locked-in to the same carrier signal frequency ω_c. Hence the name lock-in detection also applies to the method. Calling the input signals to the multiplier as X_1 and X_2, then

$$X_1 = E_c \cos \omega_c t$$

$$X_2 = E_m \cos(\omega_c t + \phi)$$

Output X_o of the multiplier will be $X_o = X_1 X_2 = E_c E_m \cos\omega_c t \cdot \cos(\omega_c t + \phi)$.

$$X_o = \frac{E_c E_m}{2} [\cos \phi + \cos (2\omega_c + \phi)] \qquad (4.1)$$

If we filter the output of the multiplier such that $\omega_{cutoff} << 2\omega_c$ then

$$X_o = \frac{E_c E_m}{2} \cos \phi \qquad (4.2)$$

If in eqn. (4.2) now, a phase shifter is introduced in the reference channel such that phase difference between the two signals X_1 and X_2 is zero, then

$$X_o = \frac{E_c E_m}{2} \qquad (4.3)$$

Hence if the 'system under test' is so designed that changes in capacitance are reflected as amplitude modulation of E_m, then X_o the output signal will be proportional to capacitance

changes directly and we have succeeded in getting capacitance transients.

4.3.2 Design of Setup:

Keeping the above block diagram of Fig. 4.2 in mind, the capacitance measurement module should look like as in Fig. 4.3. A brief discussion of each block is given along with the realization.

a) Summer: Summer is needed to sum up three quantities:

1. Pulse bias 2. D.C. bias (for minority carrier pulse) 3. High frequency sinewave.

As operation needs to be done at high frequencies, LM318/CA3140 were found suitable for this application.

b) I/V converter: The design of this is the trickiest, since the signal level is quite low here and this being the first stage following Fritz's law, it needs to be as noise free as possible. It is instructive to know the order of currents available to be amplified by this converter.

Amplitude of carrier signal = 10 mV

Frequency of carrier signal = 500 KHz

Typical capacitance of 1N4148 diode (from data sheets) = 4 pF

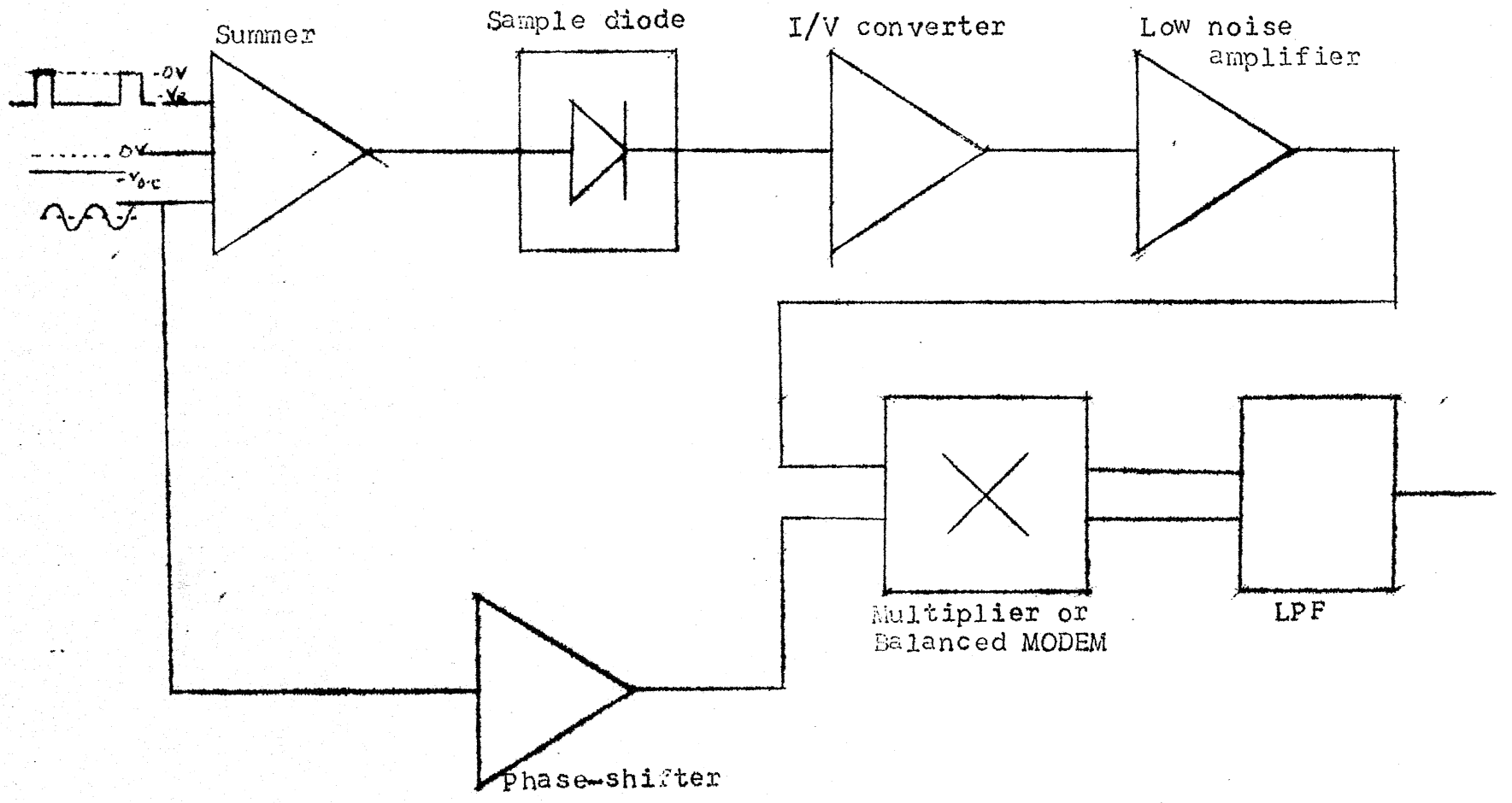

Fig. 4.3: Schematic of capacitance measurement module

Capacitive reactance of the diode

$$= \frac{1}{2\pi \times 500 \times 10^{3} \times 4 \times 10^{-13}}$$

$$= 80K$$

$$\text{Current through the diode} = \frac{10 \times 10^{-3}}{80 \times 10^{3}}$$

$$= 100 \text{ nA}$$

This current has to be converted to voltage at 500 KHz and further amplified. The noise itself can be in millivolts and hence one needs to be careful. Here this is obtained by following steps:

a) This low current is dropped across a precision resistor. The value of this resistor is so chosen that it is much smaller than the impedance of diode in reverse bias and at that frequency.

b) The developed voltage is then buffered using a very low noise and excellent high frequency voltage follower LM310.

c) The buffered voltage is then amplified using a wideband amplifier (HP model 461A), having excellent input characteristics. However only gain of 10 is possible because amplifier oscillates due to mismatches at output.

d) The signal level still is low and hence the oscilloscope vertical amplifier output itself is taken. This output is applied to the multiplier block as one of its inputs.

C) Phase shifter: It is achieved using CA3140 in a phase-shifter configuration and is detailed in the actual circuit diagram.

D) Multiplier: The process of multiplication can be done using either a four quadrant multiplier or a balanced modulator. However the disadvantage with the available balanced modulators is that output signal level is small and hence further amplification is needed. Hence a four-quadrant multiplier XR-2208 is used in its phase-sensitive detection mode as shown in Fig. 4.4.

V_ϕ in this case is given by:

$$V_\phi = K_d \cos \phi$$

where K_d is the phase detector conversion gain. If $K_d \geq 50$ mV r.m.s., $K_d = 2V/\text{radian}$. However, if input signals are <50 mV rms, then K_d changes as the input changes. However, the output from Fig. 4.4 is differential in nature and hence a difference amplifier must follow. Again LM318 was found quite satisfactory for this purpose.

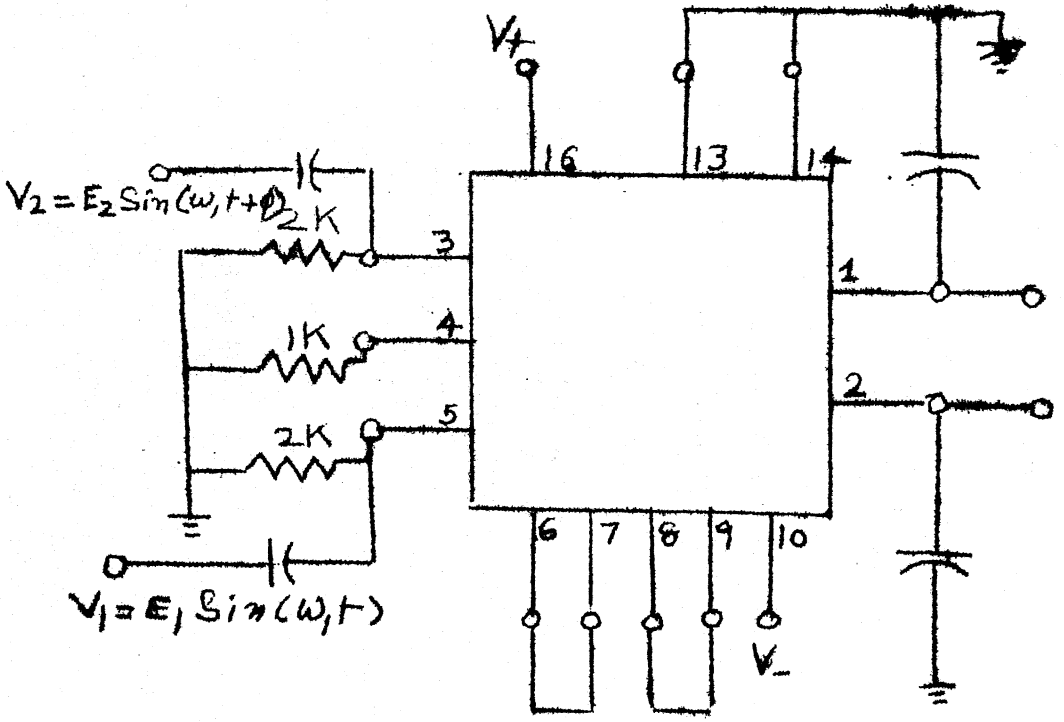

Fig. 4.4: XR-2208 as phase sensitive detector.

Since K_d is small, its amplitude is increased by amplifying the reference signal in reference channel since any way on that channel, signal has to be larger than 50 mV r.m.s. The signal circuit then looks like as in Fig. 4.5.

4.4 DESIGN OF CURRENT TRANSIENT MEASUREMENT MODULE:

Current transient measurement module has two features different from that of capacitance measurement module in previous section. One is that one need not work at high frequencies in this case and second that level of signals is smaller in this case than of capacitance transients. The latter is particularly true since now it is the reverse bias current, which has to be monitored. In silicon diodes, this current is of the order of a few nanoamperes. Again due to requirements of Fritz's law, the first current to voltage converter should be as noise free as possible. The block diagram of such a setup is in Fig. 4.6. A brief description of each block is provided.

a) I/V Converter: This stage should be as noise free as possible. Hence a FET input low noise OPAMP is used. CA3140 is characterized by low offset voltage, low offset current high CMRR and high input impedance. Several stages of transimpedance are provided.

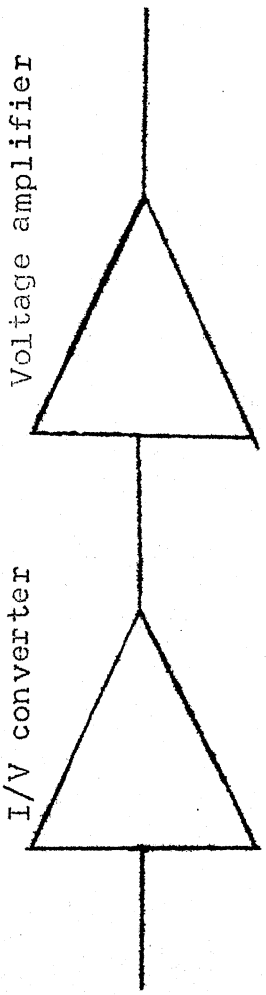

Fig. 4.6: Block diagram of current measurement set up.

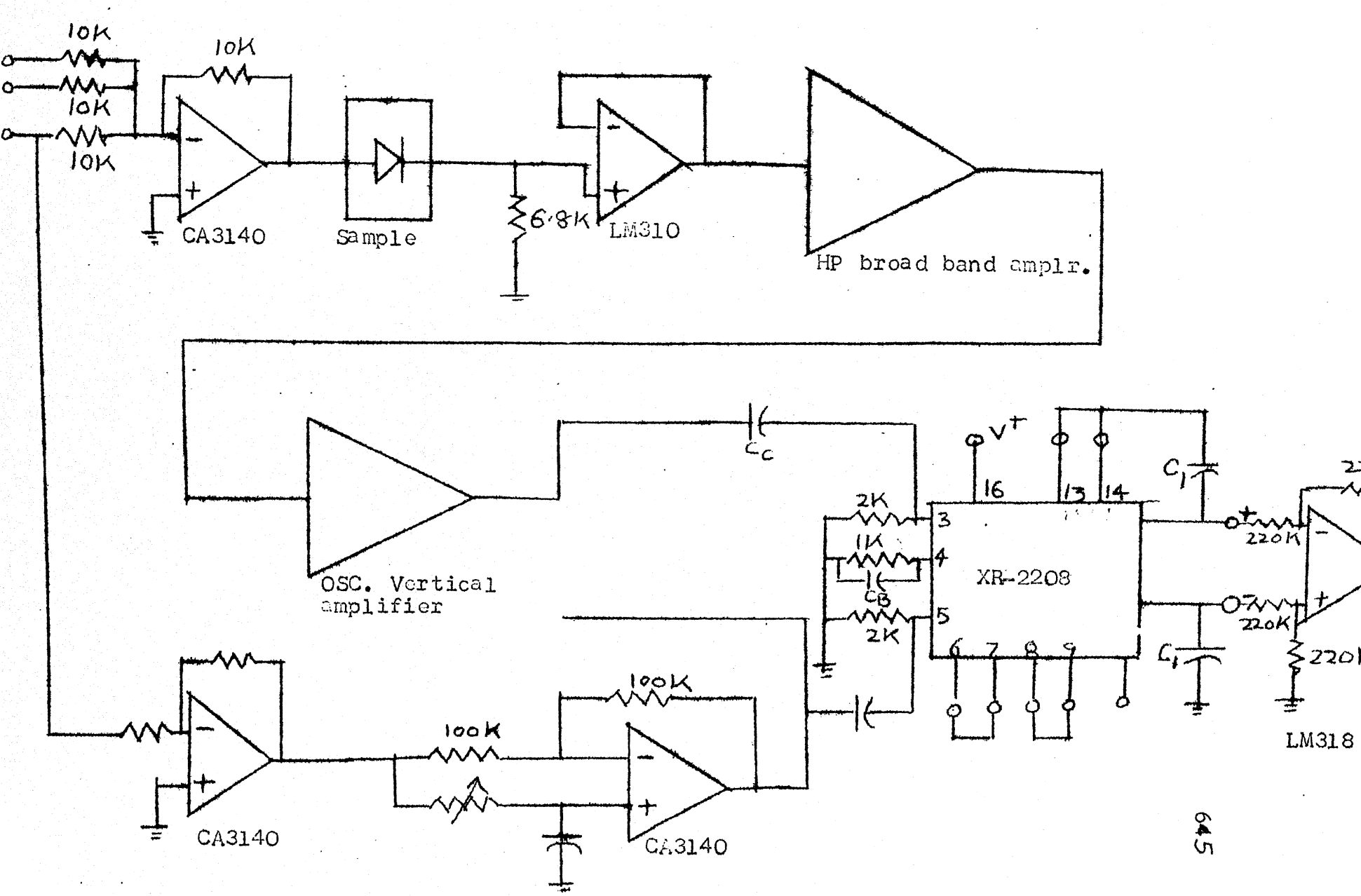

Fig. 4.5: Final circuit diagram for capacitance transient measurement

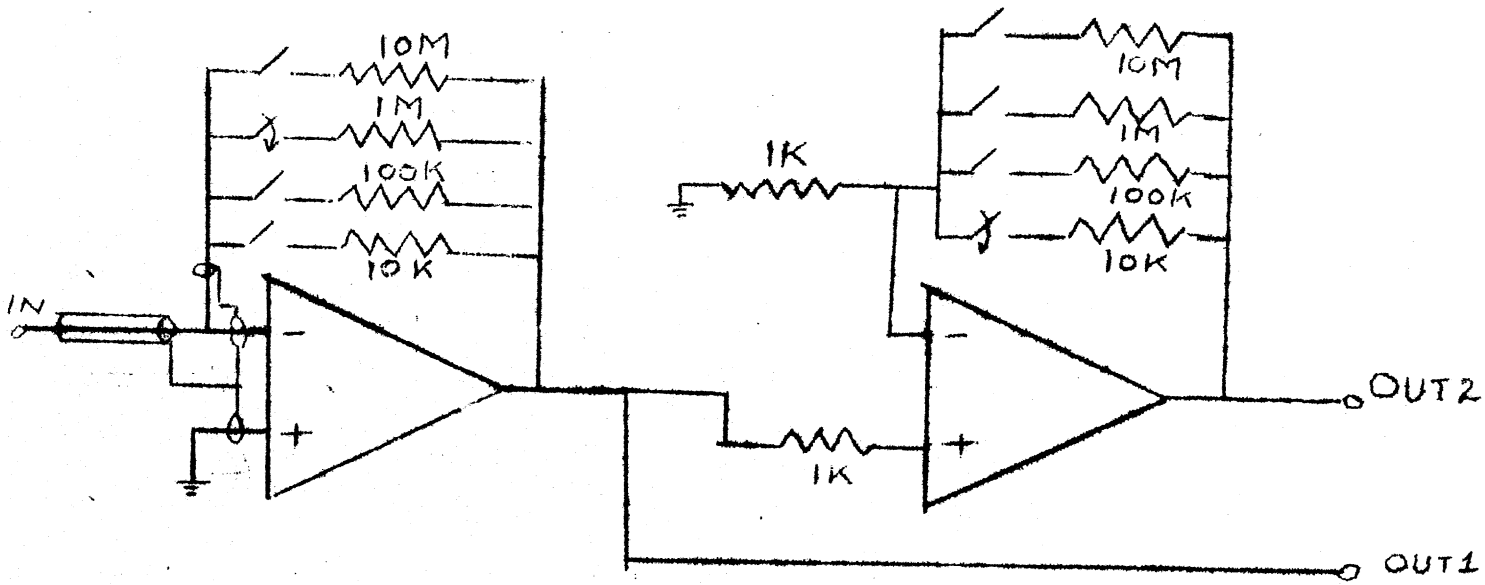

Fig. 4.7: Final current transient measurement circuit

b) Voltage amplifier: Again an amplifier with low noise, low offset current and voltages should be used. Multiple gains are provided in this case, too.

The final current transient circuit is as shown in Fig. 4.7. Some very important precautions need to be taken regarding:

a) layout and connections

b) selection of passive components

For layout, the above low noise, low level current transient set-up or electrometer should have proper shielding and guardrings must be provided to avoid loss of signal [13,14]. Both capacitance and current transient signal measurement setups have been developed and used to acquire these transients from a $P^{+}N$ junction diode. The details of this are in Chapter 5.

CHAPTER 5

EXPERIMENTAL RESULTS AND DISCUSSION

5.1 INTRODUCTION:

In this chapter the details of current and capacitance transients from commercially available Gold doped P^+N junction diode have been given. These transients have been analysed to obtain the values of activation energy and capture cross-section related to Gold acceptor in silicon. The details are described below:

5.2 CURRENT TRANSIENTS:

The experimental system used to measure current transients has already been described in Fig. 4.1. A total of eighteen such transients spanning a temperature range of 110°K from 236°K to 274°K are taken and those at two temperat
are shown in Fig. 5.1 and
waveshapes are similar to the theoretically predicted one in Fig. 2.4. Before analysing these for determination of activation energy and capture cross-section, following considerations, over and above those already described for the measurement system of Fig. 4.1 are taken.

1. Each of the transients is measured using a majority carrier pulse wherein the voltage switches from O V to a reverse voltage $-V_R$. To illustrate the shape of pulse bias, the

majority carrier pulses in case of transients at T = 251°K and T = 274°K are shown in Fig. 5.1.

2. It has been found that pulse bias at a single frequency cannot be used for the complete temperature range used. This is because at lower temperatures, the time of decay of current transients are so large that it does not totally become zero, leading thus to conditions for DDLTS (Double DLTS). In such a case the analysis needs to be changed accordingly. On the other hand at high temperatures, the decay is so fast that a set of indistinguishable transients are obtained close to the negative going transition of bias pulse. Therefore for higher temperatures, high repetitive rate pulses are used and for lower temperatures, the repetitive rate is made so large that the decay is complete. This particular point is illustrated in Fig. 5.1 where the transient at T=274°K is measured using a pulse of about 2.40 ms period and one at T=251°K obtained with about 85 ms pulse period.

The transients obtained are submerged in noise. Hence the signal averaging capability of the signal analyser is used to increase SNR for these transients and it has been found that at least five hundred such averagings are necessary.

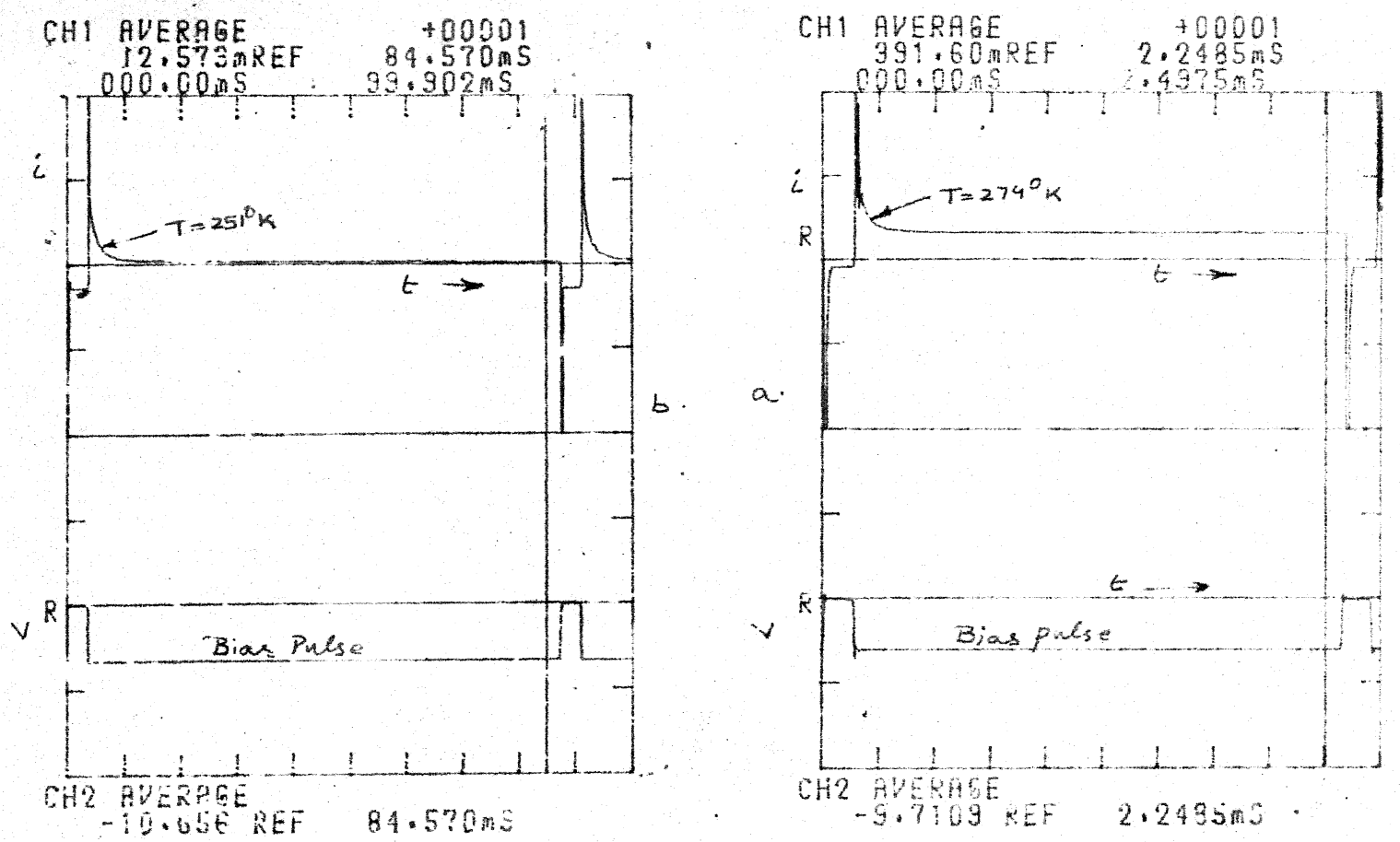

Fig. 5.1: Current transients at two different temperatures on a given majority carrier pulse sequence.

Before analysing the data, it is necessary to check out some features of current transients which are predicted by the eqn. (2.26). These are:

a) that the decay constants of the current transients decrease with decreasing temperature and

b) that the initial amplitude becomes smaller as the temperature is lowered.

Property (a) above is verified in Fig. 5.2 where the current transient signals at three different temperatures ($T=346^{o}K$, $325^{o}K$ and $T=306^{o}K$) have been plotted. In Fig. 5.2(a), $T=325^{o}K$ and $T=346^{o}K$ transients are compared and values are read by cursor at $t = 261.23\ \mu s$ to show a higher value of 826.43 mV for $T=346^{o}K$ transient meaning thereby that lower amplitude for latter transient is due to its faster decay. Similarly Figs. 5.2(b), 5.3(a) and (b) illustrate this property.

Theproperty (b) above can be observed by comparing the order of magnitudes of transients in Fig. 5.2 with those in Fig. 5.3. For instance at the cursor setting of $t=261.23\ \mu s$ in Fig. 5.2, the magnitudes are in hundreds of millivolts while in case of Fig. 5.3 at $t=8.0078$ ms setting of cursor, the magnitudes are in terms of millivolts. The temperatures in Fig. 5.3 are lower than temperatures in

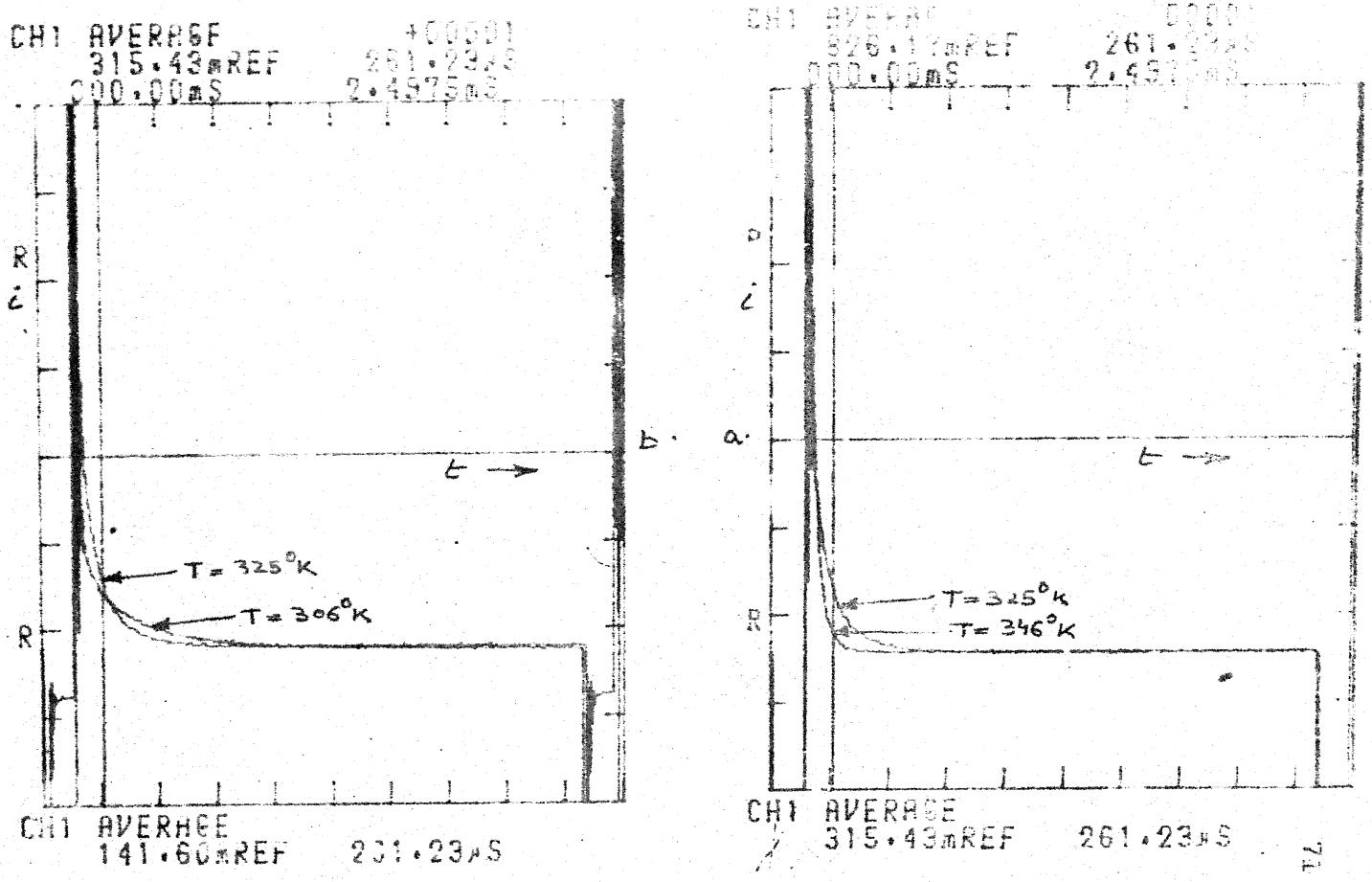

Fig. 5.2: Comparison of current transients at different temperatures on a given majority carrier pulse sequence.

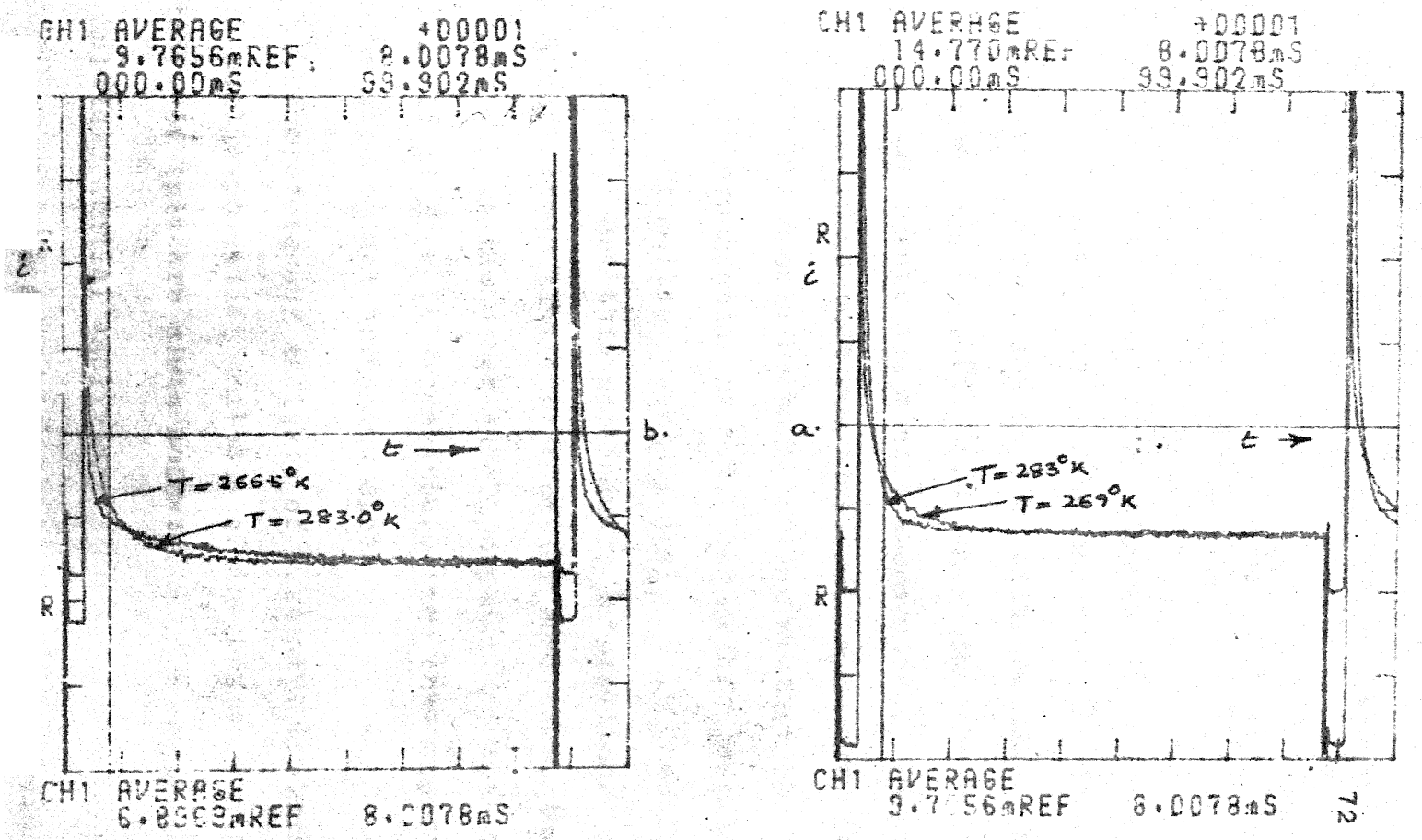

Fig. 5.3: Comparison of current transients at two different temperatures on a given majority carrier pulse sequence.

Fig. 5.2, meaning hence that amplitudes decrease with temperature.

5.2 ANALYSIS FOR CURRENT TRANSIENTS:

The eighteen transient signals experimentally obtained have been analysed for determination of activation energy and capture cross-section. Many of the methods [4], [5], [8], [10] including the DLTS assume that the transients are single exponential. In practice it has been found that sometimes multiexponentials occur. Hence efforts should be made to find whether the transients are single exponential or not. The method described in Chapter 3 for multiexponential analysis is used for the first time to get this preliminary information. In case the signal shows single exponential behaviour, then either DLTS or any of the other single exponential analyses can be used. If it is multiexponential, then this algorithm itself can be used to get Arrhenius plot.

Therefore our analysis of current transients starts with multiexponential analysis of these transients. The details of this are given below:

a. Multiexponential analysis:

Herein the analysis is done at two temperatures. The current transients at 321.63^{o}K and 258.5^{o}K are chosen for

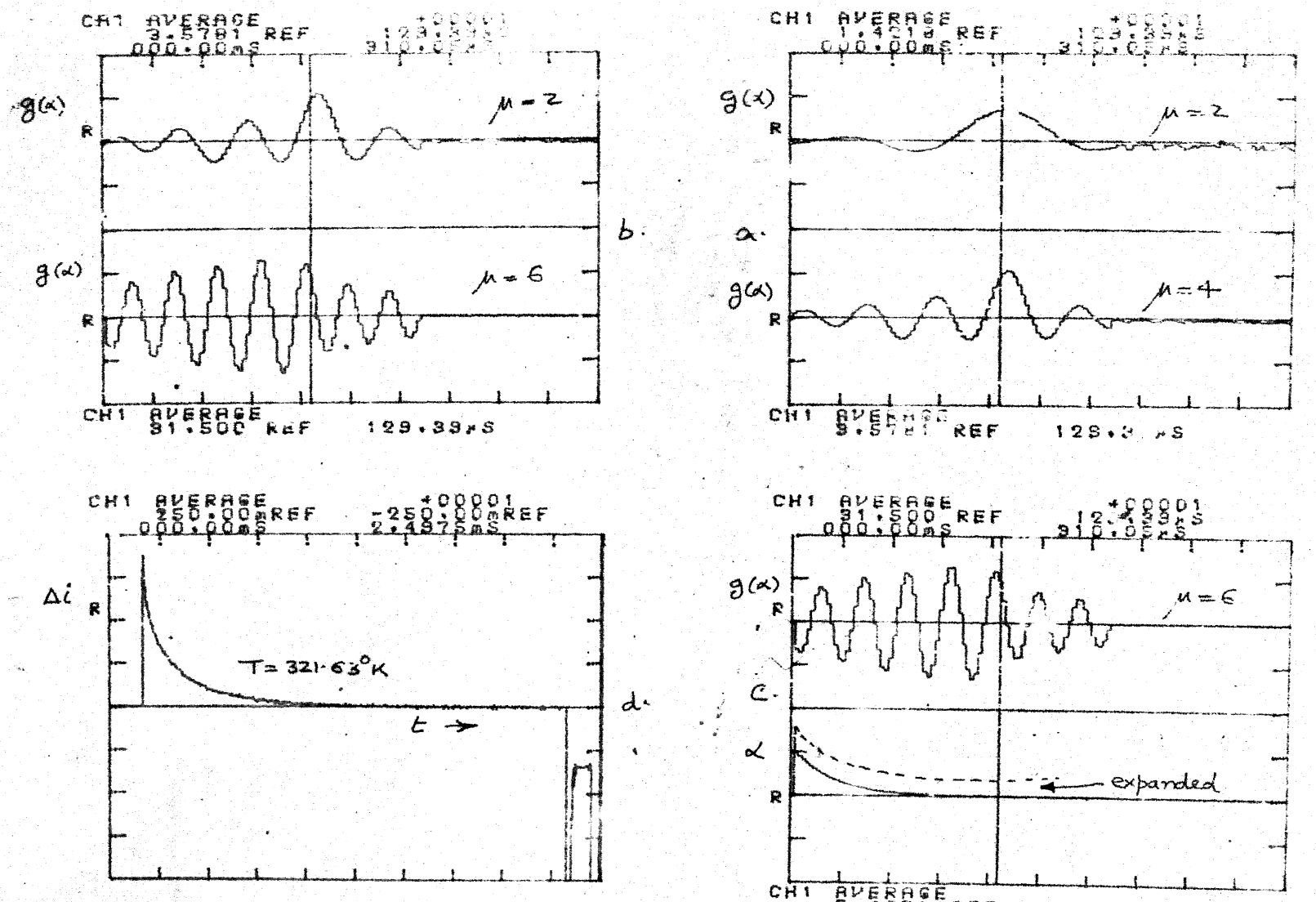

Fig. 5.4: Multiexponential analysis of current transient at T=321.63°K.

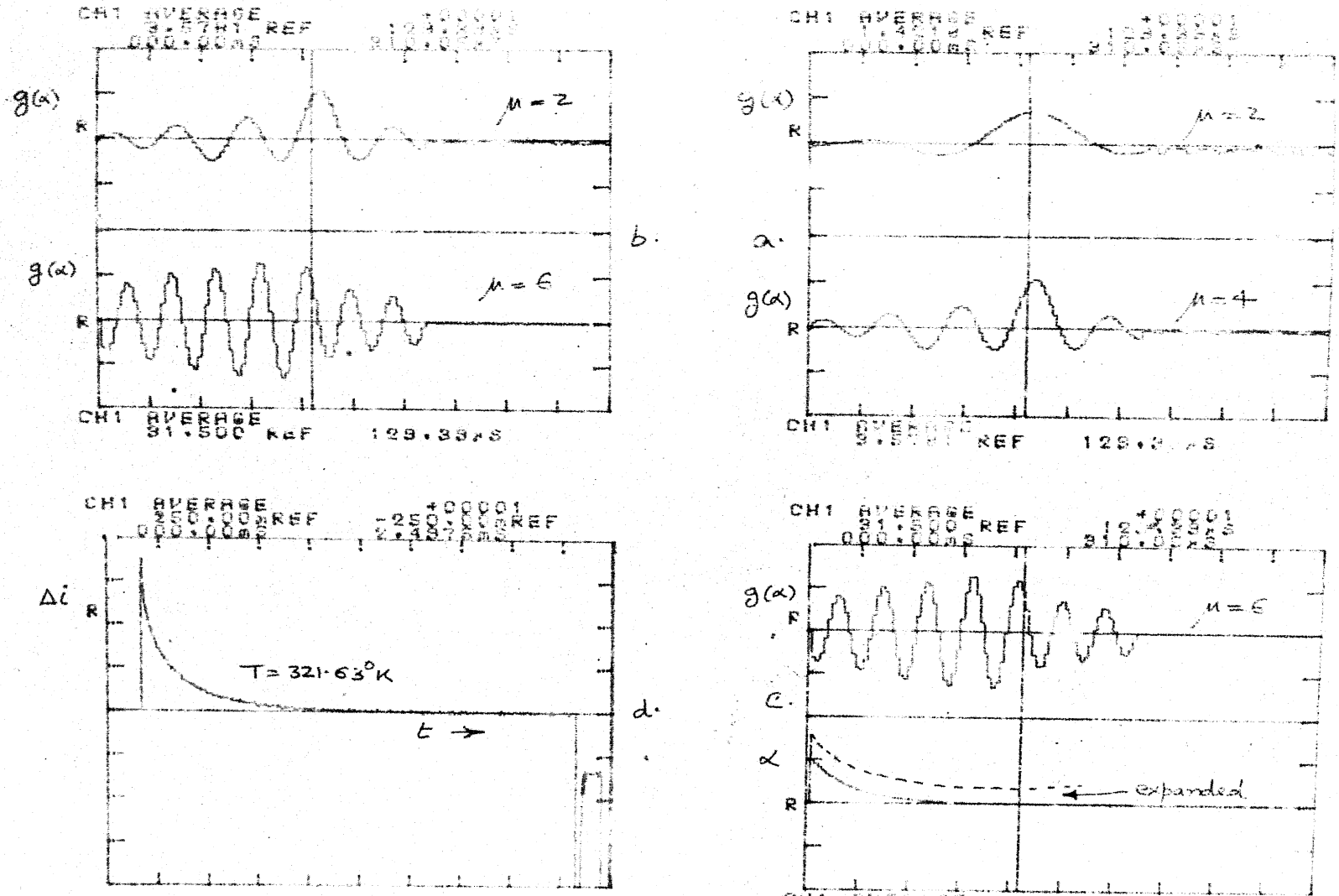

Fig. 5.4: Multicomponential analysis of current transient at T=321.63°K.

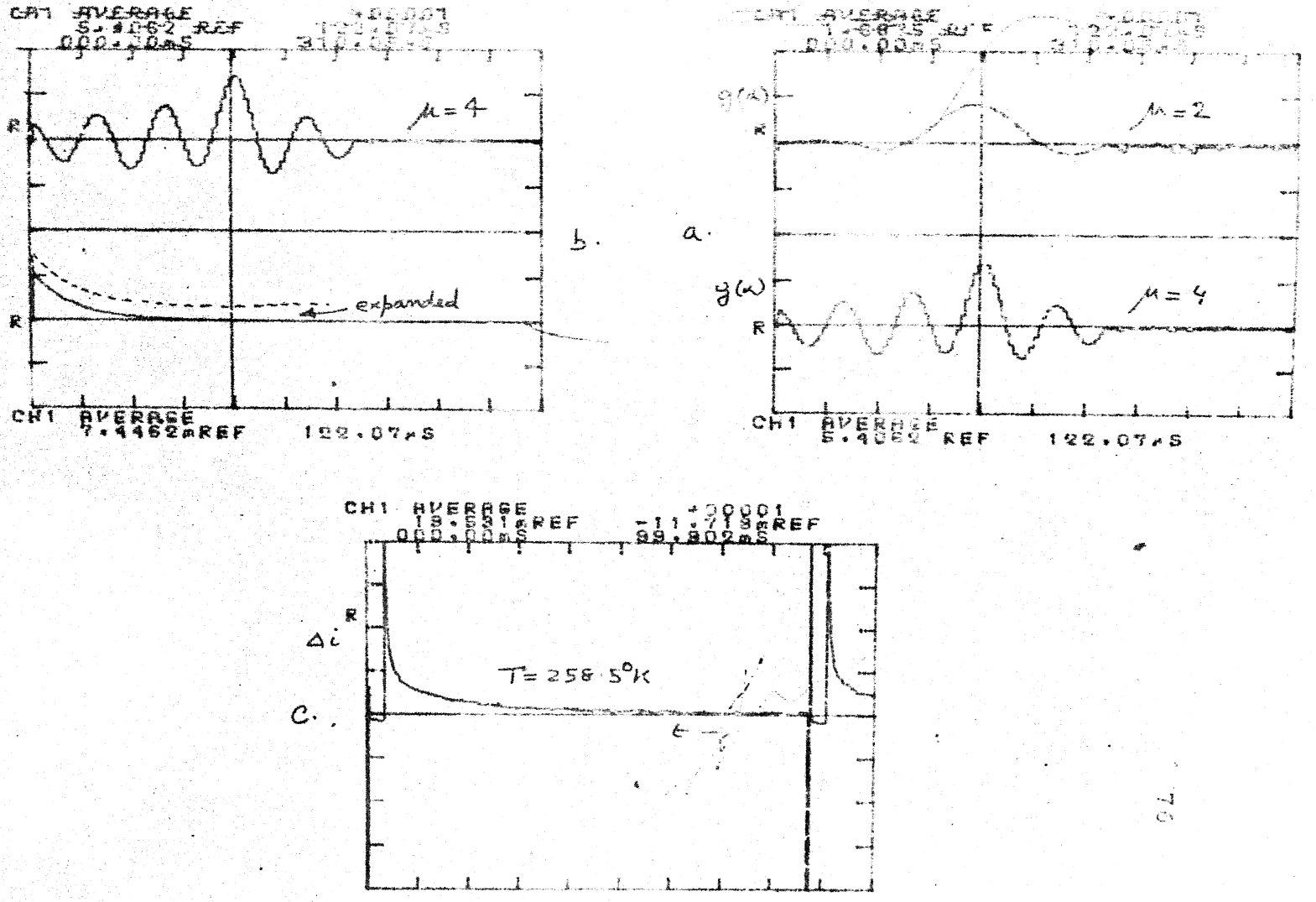

Fig. 5.5: Multiexponential analysis of current transient at T=258.5°K

specifically this effect is illustrated in Fig. 5.6(a) and (b) at two different temperatures.

2. Because of the above mentioned problem, using arguments of chapter three, area method is used to find values of B. These values for each temperature are given in Table 5.1. As can be seen, the values of B decrease with lowering of temperature, because it is due to leakage current which is temperature dependent.

3. The values of α and A are obtained from the original curve minus the value of B (i.e. $Ae^{-\alpha T}$). The program for this is provided in Appendix I. The values of A and α are also tabulated in Table 5.1. The values of both decrease with decreasing temperature according to eqn. (2.26).

4. These values of α with corresponding temperatures T are used to obtain the Arrhenius plot. As mentioned in Chapter 2, the slope of this plot gives the activation energy and intercept the capture cross-section. The values as obtained from the graph are shown therein.

5. The above values of α and 1/T are also fitted by a linear regression algorithm provided in Appendix I. The values of E, the activation energy and g σ_n, the capture cross-section are shown in Table 5.2.

Next we discuss the capacitance data:

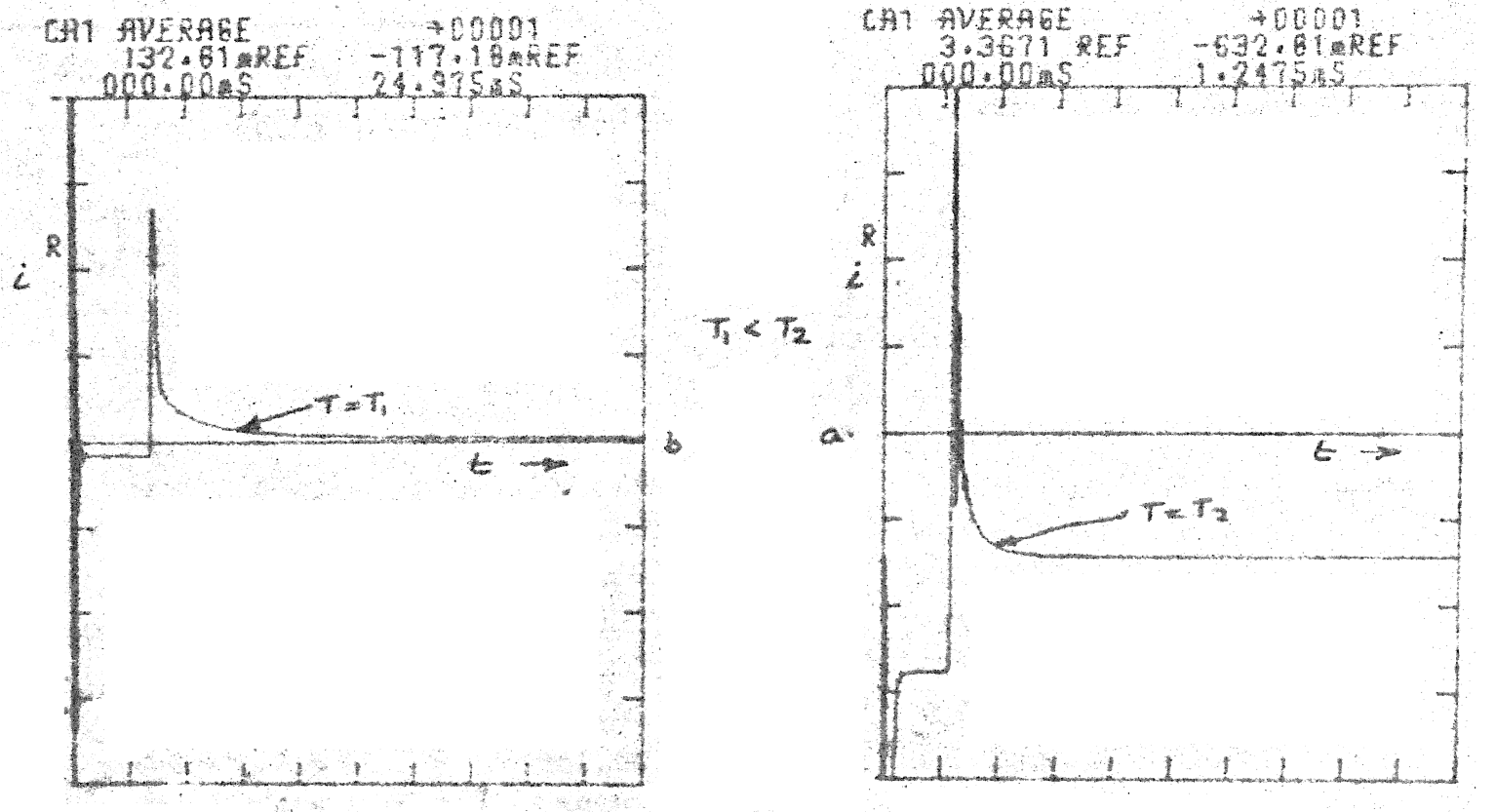

Fig. 5.6: Initial jitter in current transients.

Table 5.1: Current Transient Data

DVM reading in mV	t_o	t_{amb}=26.5°C $t+t_{amb}$ °C	T °K	α	B	A
+1.903	46.90	73.40	346.4	29929.6	+.793945	.59091
+1.750	43.41	69.80	342.8	26157.8	+.647461	.426551
+1.408	35.17	61.67	334.67	20932.8	+.395507	.416720
+1.033	26.09	52.59	325.59	13321.6	+.217285	.319616
+0.875	22.175	48.675	321.675	11984.7	+.167968	.292027
+0.747	19.0	45.5	318.5	9720.55	+.134277	.209612
+0.565	14.45	40.95	313.95	7580.39	$+.93261\times10^{-1}$	.181212
+0.437	11.20	37.70	310.7	6805.17	+.74707E-1	.159619
+0.283	7.30	33.8	306.8	5886.58	+.571289E-1	.146478
-0.087	-2.26	24.24	297.24	5130.87	+.35644E-1	.081954
-0.229	-6.00	20.50	293.50	3054.75	+.217285E-1	.074630
-0.433	-11.42	15.08	288.08	1888.84	+.129394E-1	.050473
-0.604	-16.00	10.00	283.00	699.077	+.125732E-1	.62037E-1
-0.805	-21.47	5.03	278.03	497.057	+.94909E-2	.148043E-1
-1.133	-30.58	-4.08	268.92	244.117	+.65307E-2	.747719E-2
-1.254	-34.00	-7.5	261.50	155.657	+.56152E-2	.540611E-2
-1.490	-41.00	-14.5	258.5	69.0142	+.42724E-2	.264043E-2

Table 5.2: Experimental results

	Current transients	Capacitance transients
ΔE_{ev}	0.529232	0.581456
$g\sigma_n\ cm^2$	8.84469×10^{-15}	6.64321×10^{-15}

Arrhenius plot (current transients)

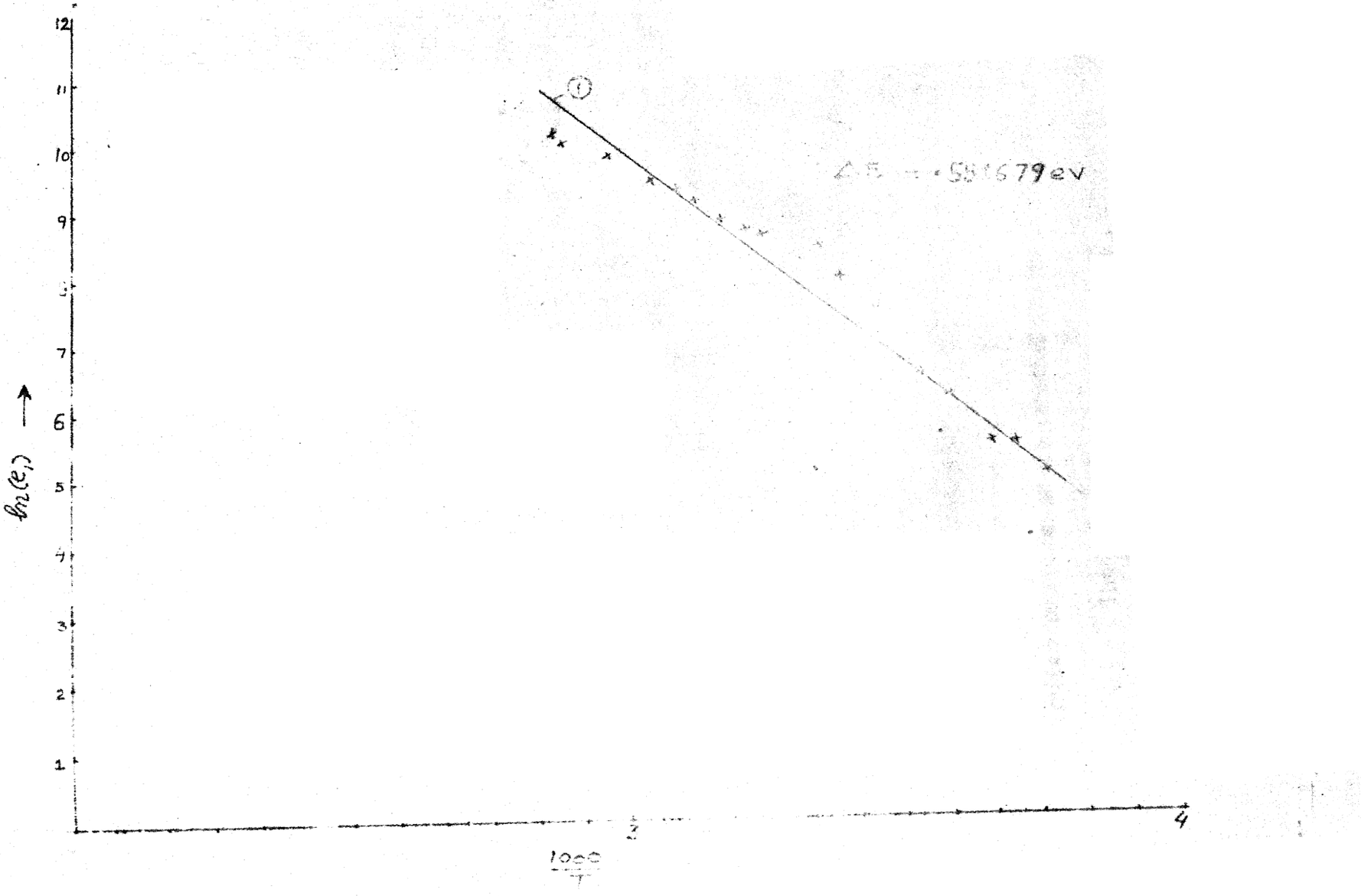

5.3 CAPACITANCE TRANSIENTS:

There is only one change while measuring the capacitance transients as compared to that of current transients. In the measurement system of Fig. 4.1, the current measurement set up is replaced by capacitance set up. A total of eleven measurements are made over a 50°K range from 298.9°K to, 250°K. The waveshape of typical capacitance transients is illustrated in Figs. 5.7 and 5.8. These waveshapes are found to be same as theoretically expected in Fig. 2.4. Both the considerations mentioned for current transients hold in this case too. This means that we have again majority carrier pulses, switching from 0 V to a reverse voltage - V_R. This is illustrated in Figs. 5.7 and 5.8, where the pulse bias is shown below the capacitive transients at four different temperatures. Due to the same difficulties as faced in current transients, a set of different repetition rates are use For the highest temperature of these at T=292.71°K the pulse period is about 9.0 ms and for the lowest temperature T = 246°K illustrated in Fig. 5.8(b), the pulse period is 90 ms. The intermediate two temperatures similarly have pulse periods of 16 ms and 45 ms.

The capacitance transients are again very noisy and at each of the temperatures multipoint averaging is done to get cleaner signal. The effect of noise is more at lower

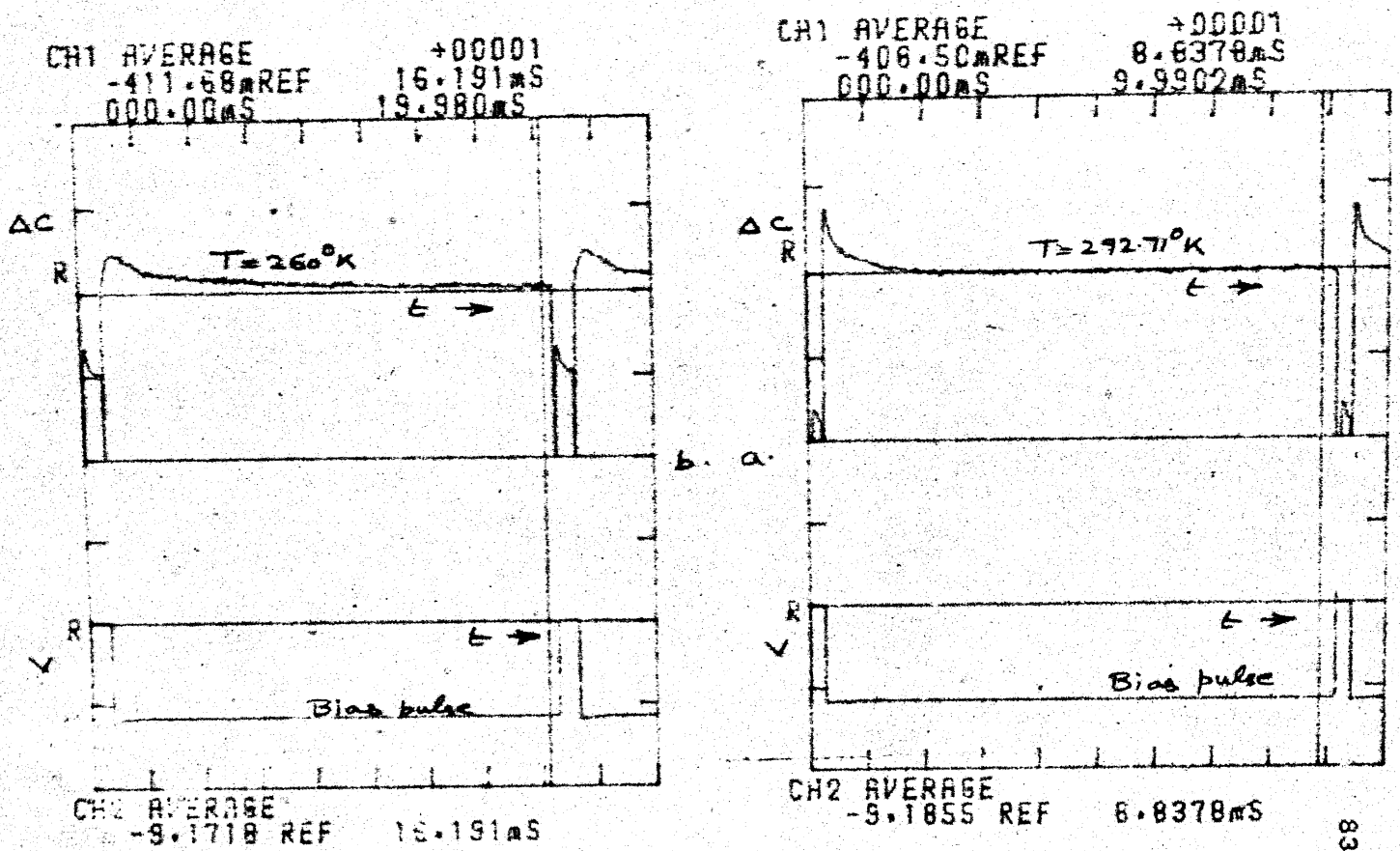

Fig. 5.7: Isothermal capacitance transients at two different temperatures on a given majority carrier pulse sequence.

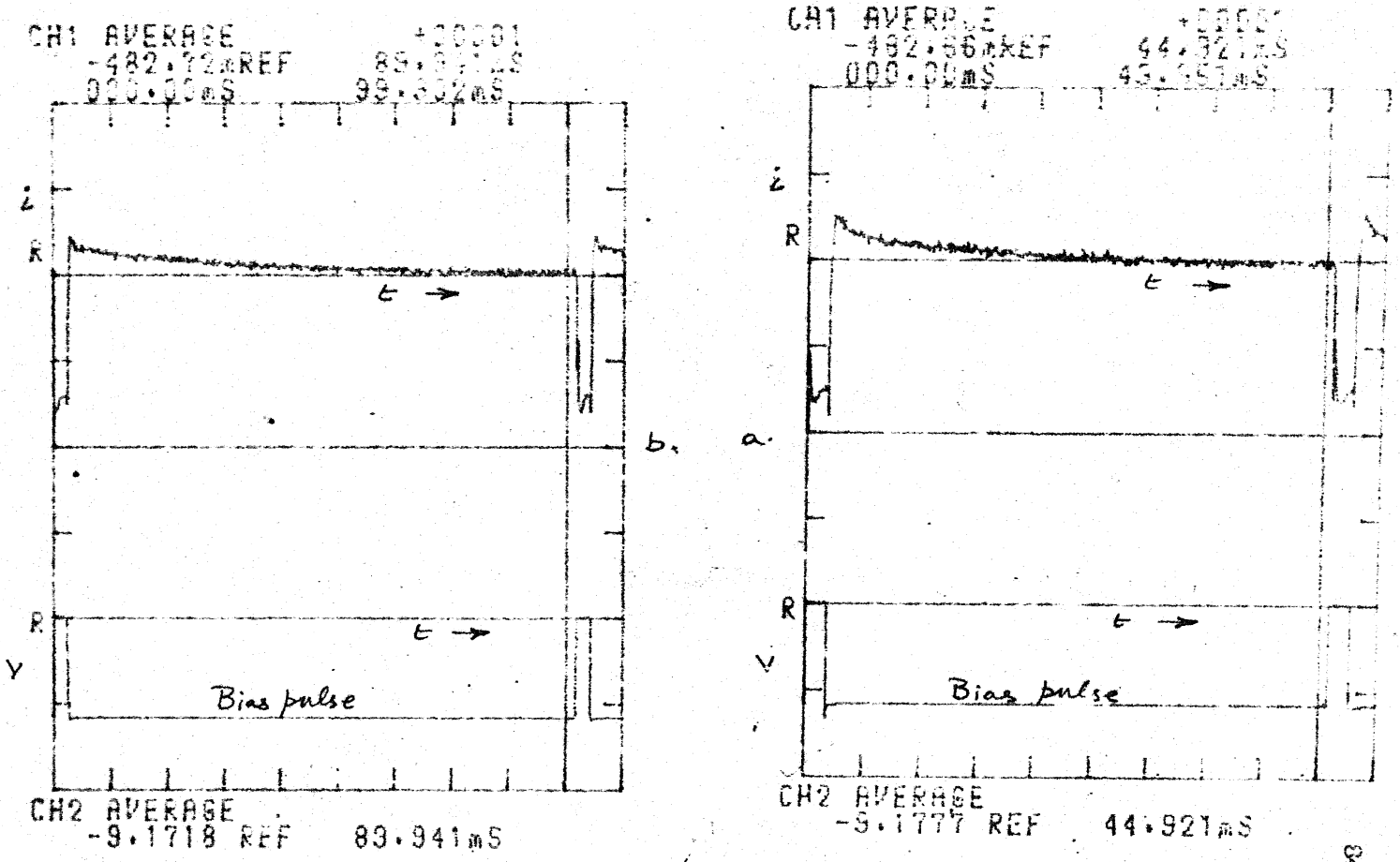

Fig. 5.8: Isothermal capacitance transients at two different temperatures on a given majority carrier pulse.

temperatures when signal strength becomes small. This effect can be observed in Figs. 5.7(b), 5.8(a) and (b) and Fig. 5.9(b).

In this case too, we check the capacitance transients for some features predicted by eqn. (2.19). These are:

a. that the decay time increases as the temperature is decreased

and b. that the initial amplitude remains constant.

Property (a) is verified in Fig. 5.8(a) and (b) and Fig. 5.9(a). In Fig. 5.8(a), the capacitive transients at T = 298.8°K and T = 288.43°K are compared with each other. At the setting of the cursor at t = 830.07 μs, the values read are 88.195 mV and 91.735 mV respectively, meaning thereby that the transient at T=298.87°K decays faster than at T=288.43°K. The same effect can be seen at other comparisons shown in Figs. 5.8(b) and 5.9(a).

Property (b) can again be verified in Fig. 5.8(a) and (b), where initial amplitudes are found equal.

We proceed next with the analysis for determination of activation energy and capture cross-sections.

5.3.2 Analysis for Capacitive Transients:

Here again as in current transients, a serious need is felt to verify if the capacitive transients are single

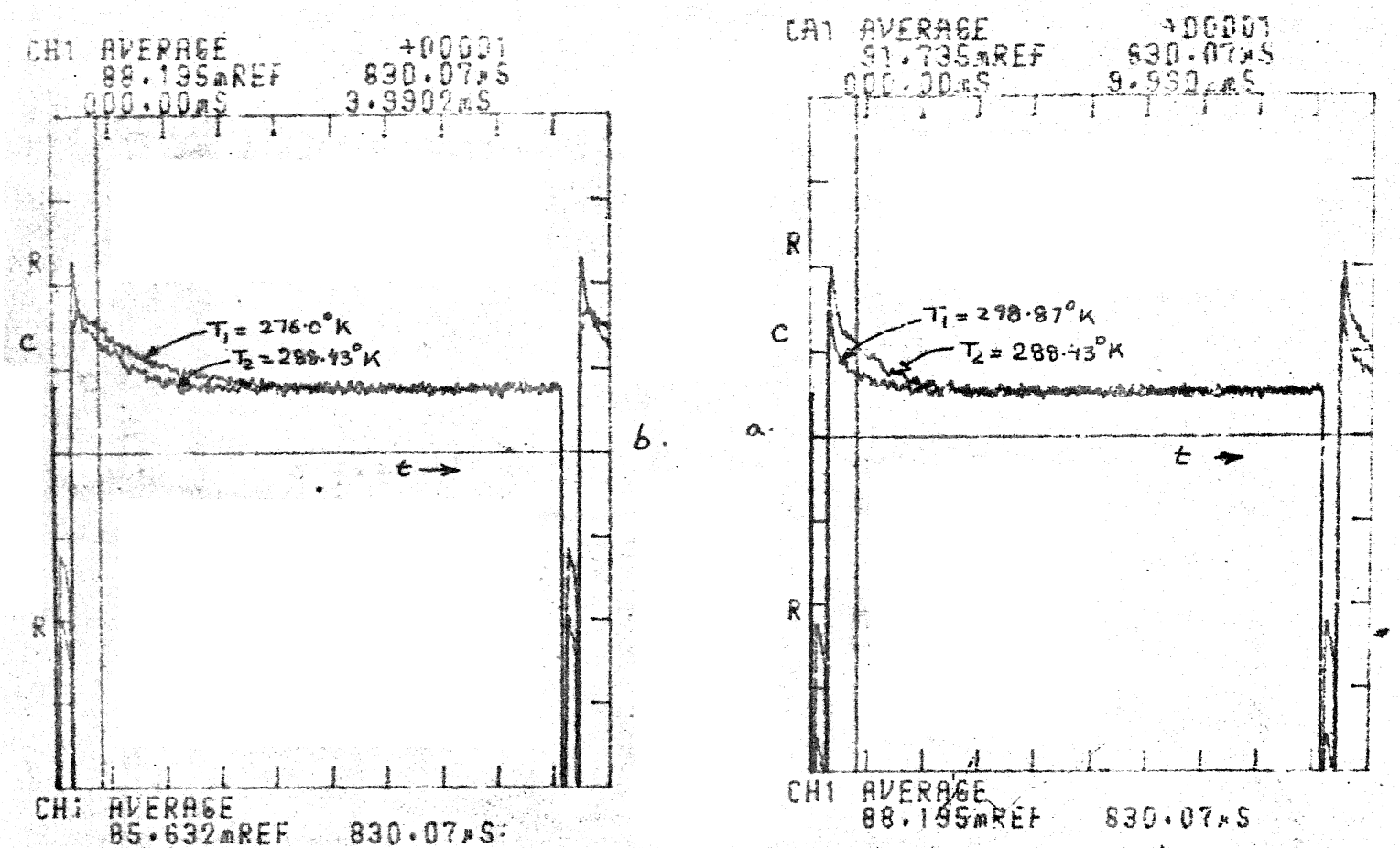

Fig. 5.8(2): Comparison of capacitance transients at two different temperatures on a given majority carrier pulse sequence.

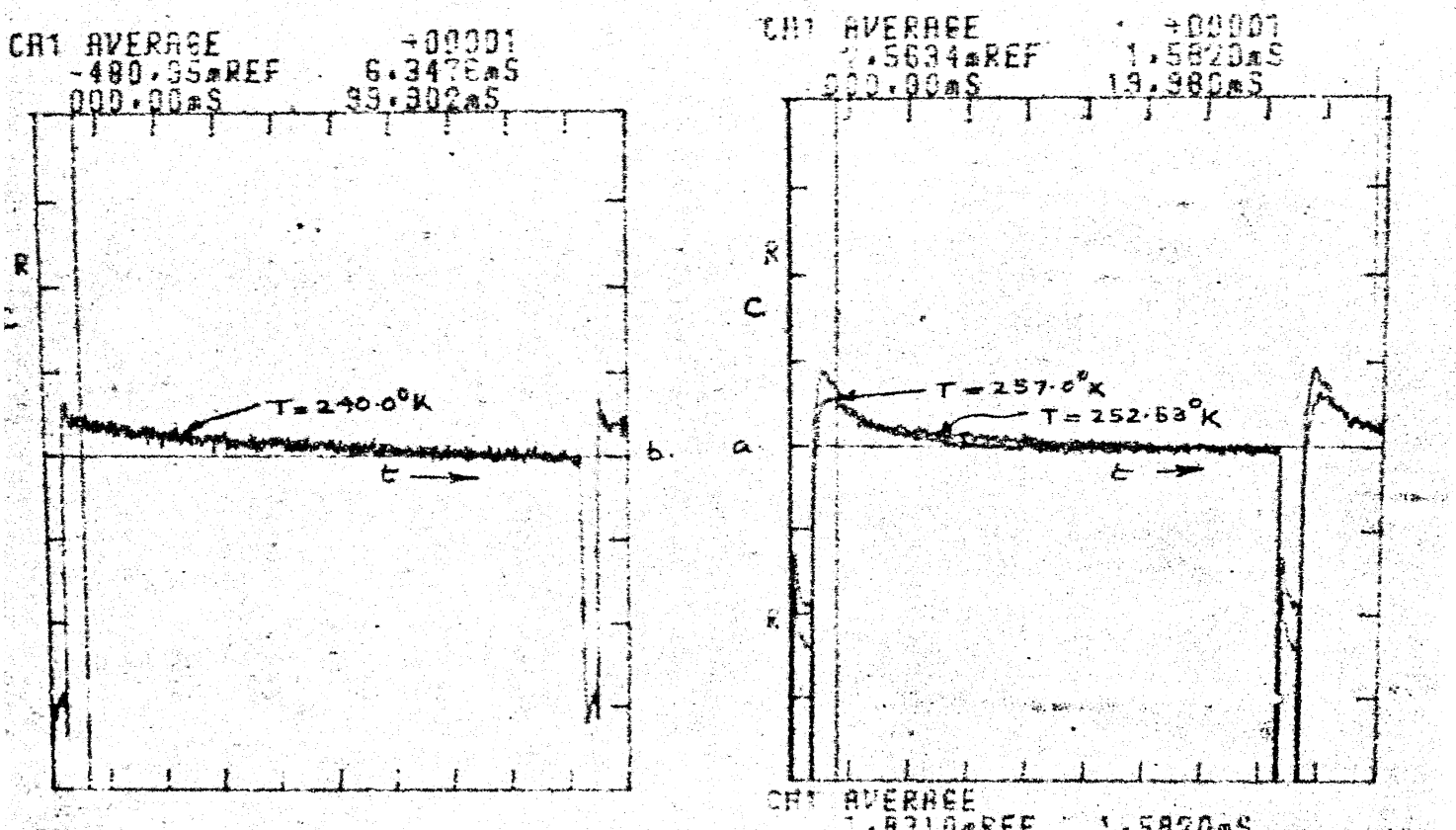

Fig. 5.9 a: Isothermal capacitance transient at T=240.0°K.
b: Comparison of two capacitance transients at two different temp. on a given majority carrier pulse sequence.

exponential or not so that either DLTS or any of the other single exponential analysis could be used or not. Therefore the multiexponential analysis is done to verify the existence of the single exponencity. In case the transients are single exponential, then either DLTS or any of the other single exponential analyses can be used. If, however, these are multiexponential, then this algorithm can be itself used to get Arrhenius plot.

Therefore our analysis of capacitance transients starts with multiexponential analysis. The details of this are given below:

a. Multiexponential analysis:

The capacitance transients at two temperatures are analysed for multiexponencity. These transient are at $T=252.53^{o}K$ and $T=279.61^{o}K$ and are shown in Figs. 5.10(d) and 5.11(c) respectively. The multiexponential algorithm when applied to transient at $T = 279.61^{o}K$ gives for $\mu=2$, $\mu=4$ and $\mu=6$ in (a) and (b) and its value can be read in Fig. 5.10(c) as 1489. This the transient at $T=279.61^{o}K$ has single exponential.

Similarly the capacitance transient at $T=252.53^{o}K$ is analysed for multiexponents. The results of this are shown in Fig. 5.11 where (a) and (b) give the$g(\alpha)$ values for

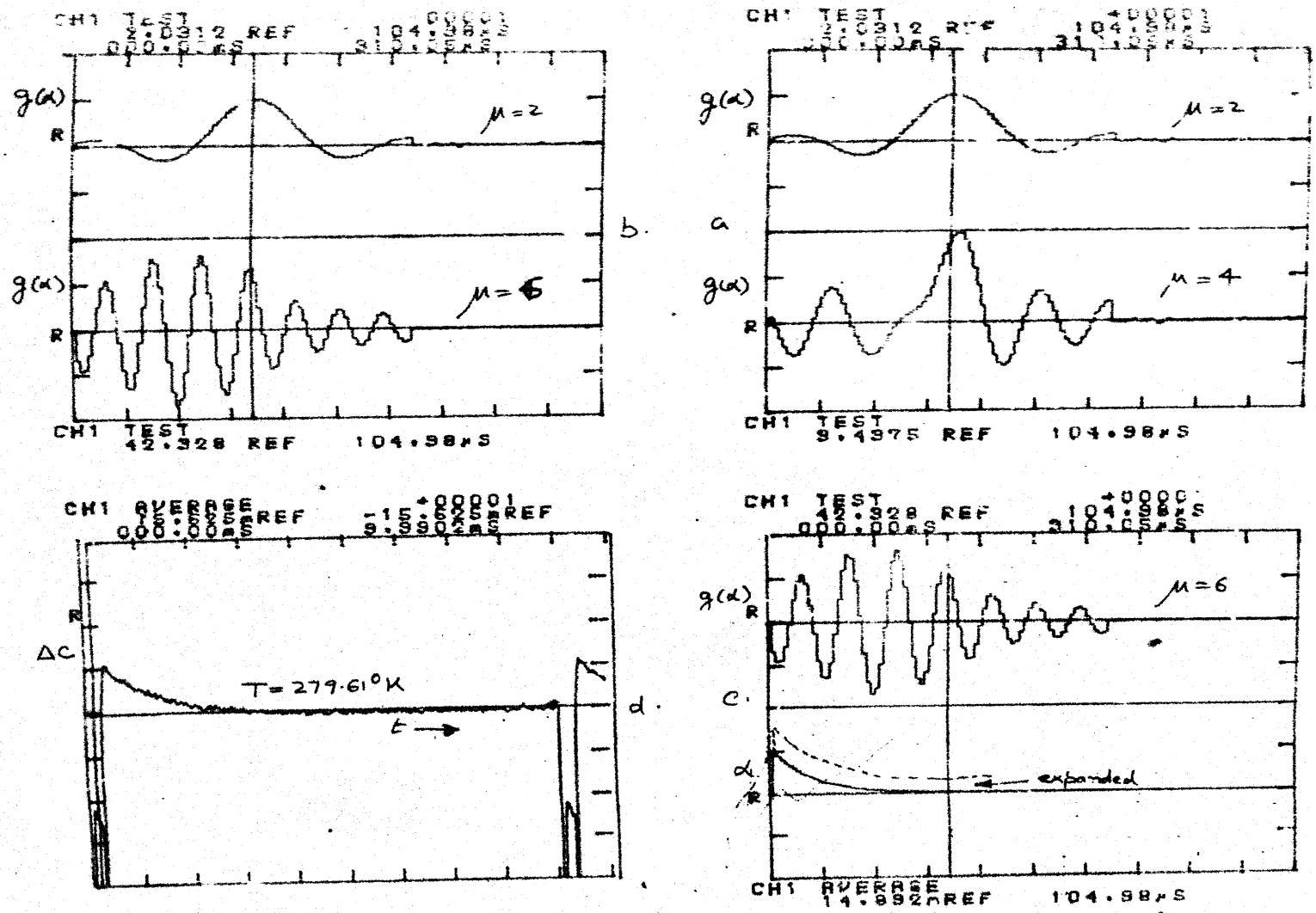

Fig. 5.10: Multiexponential analysis on a capacitive transient at T=279.61°K.

$\mu=2$, $\mu=4$ and $\mu=6$. One particular peak is seen to remain constant and the α value at this is read at the cursor point in Fig. 5.11(c). The value found for α is 135.49. Hence the capacitive transient at $T=252.53^{o}K$ is also single exponential.

The reason why only two temperatures are analysed for multicomponents is that the multiexponential analysis in its present implementation takes long time. Having verified that the transients are single exponential, any of the simpler and faster single exponential analyses can be used to find the values of decay constants. It is described below.

b. Single Exponential analysis:

Here the capacitive transients are assumed to have the form $Ae^{-\alpha t} + B$. The following steps are taken to get values of A, α and B.

1. The Area method is again used to find values of B. These values of B are tabulated for a few temperatures in Table 5.3. As can be seen that this value is essentially constant because the capacitance at steady state reverse bias is same at all temperatures. These values of B are removed from the whole waveforms at each of the eleven temperatures.

2. The modified waveforms now obtained are of the form $Ae^{-\alpha t}$ and values of α and A are determined using ratio of the

Table 5.3: Capacitance Transient Data

DVM reading in mV	t_o	$t_{amb}=25^oC$ $t+t_{amb}$ ^oC	T ^oK	α	B	A
+0.033	0.87	25.87	298.87	9000	.91475E-1	.51395E-2
-0.202	-5.29	19.71	292.71	5151	.904306E-1	.625014E-2
-0.364	-9.57	15.43	288.43	3998	.861206E-1	.60253E-2
-0.521	-13.76	11.24	284.24	2601	.86029E-1	.55721E-2
-0.692	-18.39	6.61	279.61	1640	.851276E-1	.445931E-2
- .978	-26.25	-1.25	271.75	428	-	-
-1.495	-40.94	-15.94	257.00	220	-	-
-1.651	-45.47	-20.47	252.53	138	-	-
-1.874	-52.00	-27.0	246.00	60	-	-
-2.045	-47.24	-32.24	240.76	35	-	-

Arrhenius plot (capacitance transients)

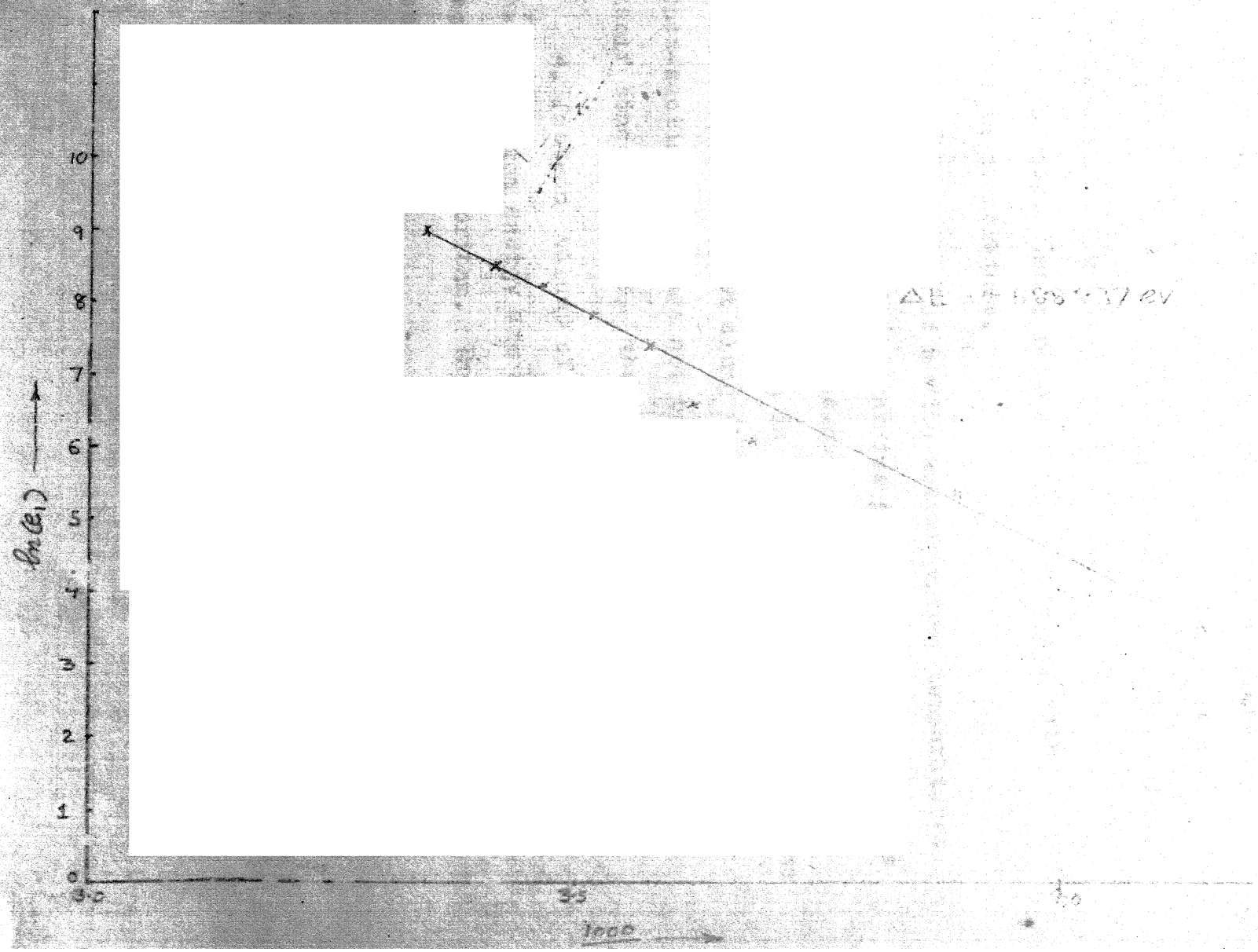

exponential function at two instants. These values of A and α are also given in Table 5.3. The value of A does show small change and it is both because of quantization error as well as the actual high frequency cut off in the signal analyser. The α values show a decrease, with decrease in temperature.

3. These values of α with corresponding temperatures T are used to obtain the Arrhenius plot. The slope of this plot gives the activation energy of the acceptor level of Gold in silicon and is given in the plot itself. Though the intercept of this plot along the ordinate gives capture cross-section, this has not been got on the Arrhenius plot itself since the plot, then extends outside the graph.

4. Instead values of the capture cross-section and the activation energy are accurately computed by linear regression algorithm. These results are tabulated in Table 5.2.

A comparison of these measured values with the ones published in literature is given in the next chapter.

CHAPTER 6

CONCLUSION

The values of the activation energy ΔE and capture cross-section $g\,\sigma_n$ of gold acceptor level in gold doped silicon P^+N Junction diode 1N4148 have been measured using majority carrier pulses. The values of ΔE using isothermal current transient study (ITS) and using isothermal capacitance transient study (CTS) have been found to be $\approx$ 0.53 eV and 0.58 eV respectively. These values are well within the published values which vary from 0.52 to 0.58 [10]. Similarly the values of $g\,\sigma_n$ found by ITS and CTS are $\approx 0.8845 \times 10^{-14}$ cm^2 and $0.664.321 \times 10^{-14}$ respectively . These $g\,\sigma_n$ values are found well within those published and which vary from $9.0 \times 10^{-17} cm^2$ to 2.5×10^{-15} cm^2 [16]

Current and capacitance transients were obtained using especially designed measurement set ups capable of acquiring low level current and capacitance signals.

A multiexponential analysis algorithm was used to help detect the multiexponents in relaxation data.

Some limitations of the above work and ways to improve these are as follows:

The multiexponential analysis, as implemented in our case, realizes Fourier transforms through numerical integrations. This means that an increase in execution time as well

as in numerical errors. If the FFT routine of the signal analyser can be used, then both the above problems can be solved.

An error analysis is particularly desirable for the multiexponential analysis. This is because the signal from the form $\sum_{i=1}^{n} A_i e^{-\alpha_i t} + B$ is reduced to $\sum_{i=1}^{n} A_i e^{-\alpha_i t}$ using Area method. The effect of such a step needs to be determined.

The multiexponential analysis has the limitation that A_i should decrease with a decrease in α_i. Due to long execution time of the program, the extent to which this condition is stringent could not be known. With FFT implementation, it would be easier then to determine the extent of this limitation.

The current transient setup could be redesigned to remove the large current component. The design is, however, slightly difficult since this fast transient decays is less than a few microseconds.

Finally the capacitance module has been found noisy. A better layout and better choice of less noisy components can help solve this problem.

APPENDIX I

I.A PROGRAM TO FIND EMISSION RATE CONSTANTS BY LINEAR REGRESSION ALGORITHM

```
  5  DIM X(500), Y(500)
  7  H = 2.4414E-06
  9  E3=50, E4=50
 10  J= = 55, J7 = 55
 12  T8 = 300
 15  T7 = 30
 17  FOR J = 1 TO T8
 20  X(J) = H*(J1-E3)
 30  T9 = B(2,0,J1)
 40  Y(J) = LN(T9)
 50  J1 = J1+1
 60  NEXT J
 65  S1 = 0, T1=0, S0=0, S2=0,T2=0
 70  FOR I=1 TO T7
 80  S1 = S1 + X(I)
 90  T1 = T1 + Y(I)
 95  S0 = S0 + X(I)* Y(I)
100  S2 = S2+X(I)*X(I)
110  T2 = T2+Y(I)*Y(I)
120  NEXT I
130  X1 = S1/T7, Y1=T1/T7, X2=S2/T7
135  Y2=T2/T7, P = S0/T7
140  P1=X2-(X1*X1), P2= Y2-(Y1*Y  )
150  M = (P-X1*Y1)/P1
160  C=Y1-M*X1
165  PRINT 'E3', E3
170  PRINT 'M', M, 'C', EXP (C)
172  T4 = 0
175  FOR L=1 TO T4
```

```
180  Y(L) = M*X(L)+C
190  I1 = EXP(Y(L))
200  I2 = B(2,0,J7)
205  G = (I2-I1)
210  T4 + T4+G*G
215  J7 = J7+1
220  NEXT L
230  R4 = T4/T8
240  PRINT 'MSE', R4
250  E3 = E3+1
260  IF E3 < = E4 GO TO 10
270  STOP
```

I.B PROGRAM TO FIND EMISSION RATE CONSTANTS BY FINDING RATIO AT TWO TIME INSTANTS

```
  5  DIM D(20)
 10  E1 = ?
 20  T0 = 2.4414E - 06
 30  K = 30
 40  X=E1
 42  I = 1
 45  Y = X+K
 60  TL = X* T0, T2, Y*T0
 70  Y1 = B(2,0,X), Y2=B(2,0,Y)
 80  X0 = LN(Y1/Y2)/(T2-T1)
 82  D(I) = X0
 85  X = X+1
 90  PRINT I, X0
100  I = I+1
110  IF I < =4 GO TO 45
185  S = 0
190  FOR J=1 TO I
210  S = D(J) + S
215  P = S/6
```

```
220  PRINT P,S
230  STOP
```

I.C LEAST SQUARE FIT PROGRAM TO RELAXATION DATA FOR ARRHENIUS PLOT

```
  5  DIM X(20), Y(20)
 10  T1 = 50.427, T2 = 44.95, T3 = 39.859, T4=33.6026,
     T5 = 27.8684
 20  T6 = 20.3684, T7 = 14.04, T8=8.04, T9=4.06,
     Q1 = -2.16, Q2 = -6.90
 30  Q3 = -12.186
 35  E1 = 9881.65, E2=7125, E3=5378. 260, E4=3653.9,
     E5 = 2397.92
 40  E6 = 1400.6834, E7=704.34, E8=384.03, E9=269.417,
     Z1 = 179.109
 43  Z2 = 125.062,Z3=84.9573
 45  K=1.0E-6
 47  T = 273
 50  X(1) = 1/(T1+T), X(2)= 1/(T2+T), X(3)=1/(T3+T)
     X(4) = 1/(T4+T)
 55  X(5) = 1/(T5+T), X(6)=1/(T6+T)
 57  X(7) = 1/(T7+T),X(8)=1/(T8+T)
 59  X(9) = 1/(T9+T), X(10)=1/(Q1+T), X(11)= 1/(QZ+T),
     X(12)= 1/(Q3+T)
 60  Y(9) = LN(E9), Y(10)=LN(Z1), Y(11)=LN(Z2),
     Y(12)= LN(Z3)
 61  Y(1) = LN(E1), Y(2)=LN(E2)
 62  Y(3) = LN(E3), Y(4)=LN(E4)
 63  Y(5) = LN(E5), Y(6)=LN(E6)
 64  Y(7) = LN(E7), Y(8)=LN(E8)
 65  S1=0, T1=0,S0=0, S2=0,T2=0
 67  S=12
 70  FOR I=1 TO 12
```

```
 80  S1=S1 + X(I)
 90  T1=T1 + Y(I)
 95  SO = SO+X(I)*Y(I)
100, S2 = S2+X(I)*X(I)
110  T2 = T2+T2+Y(I)*Y(I)
120  NEXT I
130  X1 = S1/S, Y1 =T1/S, X2=S2/S
135  Y2 = T2/S, P= SO/S
140  P1 = X2-(X1*X1), P2=Y2-(Y1*Y1)
150  M = (P-X1*Y1)/P1
160  C = Y1-M*X1
170  PRINT 'M', M,'C',C
175  D=M*8.61E-5
177  V = (EXP(C))/(2.6E+26)
180  PRINT 'D', D, 'V', V
190  STOP
```

I.D PROGRAM TO FIND EMISSION RATE CONSTANTS USING RATIO METHOD

```
  3  E1 = 56, E2=74, E3=98
  5  TO = 2.4414E-6
  7  T1=TO*E1, T2=TO*E2, T3=TO*E3
 10  K=8
 12  Y1=B(K,0,E1), Y2=B(K,0,E2), Y3=B(K,0,E3)
 20  XO = 1000.0
 30  P1 = (EXP(-XO*T1))
 40  P2 = (EXP(-XO*T2))
 50  P3 = (EXP(-XO*T2))
 70  F1=T2*P2*(P1-P3)
 80  F2 = T1*P1*(P3-P2)
 90  F3 = T3*P3*(P2-P1)
100  D1 = (P3-P2)*(P3-P2)
110  D2 = (F1+F2+F3)/D1
```

```
120  E2 = ((P2-P1)/(P3-P2))
130  N1 = ((Y2-Y1)/(Y3-Y2)
140  N2 = E2-N1
145  R2 = N2/D2
150  X1 = (XO-R2)
152  PRINT X1,N2
155  V = ABS (XO-X1)
160  IF V < 1.0E-3 GO TO 190
170  XO = X1
180  GO TO 30
190  R = X1
200  PRINT R
210  STOP
```

I.E PROGRAM TO FIND EMISSION RATE CONSTANTS BY AREA METHOD

```
  5  E1 = 583, E2 = 1003
 10  M=3
 12  H = 2.4414E-6
 15  J = E1, P=E2-1, K=1, E=0,    = 0
 17  F1 = B(M,0,E1)+B(M,0,E2)
 25  IF K=(INT(K/2))*2 GO TO 50
 30    =    + B(M,0,J)
 40  GO TO 55
 50  E = E+B(M,0,J)
 55  J = J+1, K=K+1
 60  IF J < = P GO TO 25
 65  PRINT 'E', E, '  ' ,
 67  PRINT 'F1', F1
 70  S = (F1+2*E+4*  ) * (H/3.0)
 80  PRINT S
 90  K = ABS (S)
100  M1= B(M,0,E1)
```

```
105  M2 = B(M,0,E2)
110  R3 = K/M1
120  XO = 0
125  T1 = E2*H-E1*H
130  F1 = EXP (-XO*T1)
140  M3 = M1-M2
145  P2 = M3*(1-XO*T1-P1)
150  P3 = (1-P1)*(K-M1*T1)*XO
155  R2 = (M3/(1-P1)
162  V2 = M1-V1
163  PRINT XO, R2,V2
165  XO = XO+500
170  IF XO < = 1.0E+5 GO TO 130
180  STOP
```

I.F PROGRAM TO FIND EMISSION RATE CONSTANTS BY RATE WINDOWING CONCEPT

```
 10  DIM D(60,20), W(60)
 20  J = 1, D1=2.4414E-6, L=1
 25  J = 1, X=5, N=1.5, N1=2
 60  FOR I=1 TO 8
 65  PR. J
 70  FREAD (I,J)
 80  J = J+1
 90  NEXT I
100, E1=132, E3=119
110  E4=364
120  M=1
130 E1=E1+X
140  E2=N*(E1-E3)+E3
150  T1 = D1*(E1-E3): T2=D1*(E2-E3)
160  TO = ((T1-T2)/LN(T1/T2))
170  W(L) = 1/TO
180  FOR K=1 TO 8
190  P1 = B(K,0,E1)-B(K,0,E2)
```

```
200  D(L,M)=P1/B(K,0,E3)
210  M = M+1
220  NEXT K
230  L = L+1
235  PR. 'N1', N1
240  IF E2 < = E4 GO TO 270
250  N1 = N1-1
260  GO TO 280
270  IF N1 > =2 GO TO 120
275  IF N1=1 GO TO 355
280  IF N1=0, GO TO 370
290     FOR M1=1
295  PRINT J
300  FREAD (M1,J)
310  J=J+1
320  NEXT M1
330  L=1
340  E1=132, E3=119
350  E4=364, M=9
360  GO TO 130
370  S = 1
380  PR. 'WINDOW', W(S)
390  FOR N=1 TO 12
391  S5=0
392  FOR S2=1 TO  150
394  S5 = S5+1
396  NEXT S2
400  PR. N,D(S,N)
420  NEXT N
430  S = S+1
440  IF S < = L GO TO 380
450  STOP
```

APPENDIX II

PROGRAM TO FIND MULTIEXPONENTS IN A DECAY TRANSIENT FROM RELAXATION STUDY

```
10 REM **********
20 REM PROG. FOR MULTIEXPONENTS
30 REM **********
40 DIM X(100), Y(100)
45 DIM Z(225),T(225)
50 X(1) = 1.000: X(2)=0.9902145: X(3)=0.9619537
   X(4) = 0.9182789.
60 X(5) = 0.8633796: X(6) = 0.8016901: X(7) = 0.7371572
   X(8) = 0.6728157
70 X(9) = 0.61081 : X(10) = 0.5523: X(11) = 0.4980:
   X(12) = 0.4480.
80 X(13) = 0.4022: X(14) = 0.36036: X(15)= 0.32210
   X(16) = 0.28713
90 X(17) = 0.25513: X(18)= 0.2258: X(19) = 0.19801
   X(20) = 0.17440
100 X(21) = 0.1519: X(22)=0.13138: X(23) = 0.11272
   X(24) = 0.0958
110 X(25) = 0,08055: X(26) = 0.06687: X(27)=0.05470
   X(28) = 0.043925
120 X(29) = 0.03449: X(30) = 0.02631: X(31) = 0.0193(
   X(32) = 0.01335.
```

```
130 X(33) = 0.00840: X(34)=0.00434: X(35)=0.00109 :
    X(36)= -0.001446.
140 X(37) = -0.00335: X(38)= -0.004713: X(39)= -0.005609:
    X(40) = -0.0061.
150 X(41) = -0.006305: X(42)= -0.006239: X(43)= -0.005978
160 X(44) = -0.005572: X(45)= -0.00506: X(46)= -0.0045017:
    X(47) = -0.0039079.
170 X(48) = -0.0033124: X(49)= -0.0027360: X(50)= -0.0021946
    X(51)= -0.0017.
180 X(52) = -0.001258: X(53)= -0.00087: X(54)= -0.00549:
    X(55) = -0.0002819.
190 X(56) = -0.0000687: X(57)= -0000946: X(58)= 0.0002131:
    X(59) = 0.0029.
200 X(60) = .0003392: X(61) = .0003588: X(62)= .0003569:
    X(63) = .0003390.
210 X(64) = .0003096: X(65) = .0002729: X(66)= .0002323:
    X(67) = .0001906
220 X(68) = .0001501: X(69) = .000112:
230 X(70) = .0000785: X(71) = .0000493:  X(72)= .0000250:
    X(73) = .0000055.
240 X(74) = -.0000093: X(75)= -.0000199: X(76)= -.0000266.
250 X(77) = -.0000303: X(78)= -.0000313: X(79)= -.0000304
260 X(80) = -.0000280: X(81)= -.0000247
```

```
270  Y(1) = 0.0000: Y(2)= =.0.0368213: Y(3)= -.0.108484:
     Y(4) = -0.150849

280  Y(5) = -.lo145: Y(6)= -.loo64: Y(7)= -.20619:
     Y(8) = -.20288.

290  Y(9) = -.19177: Y(10) = -.175144: Y(11)= -.1549509:
     Y(12) = -.132851.

300  Y(13) = -.110161: Y(14)= -.087884: Y(15)= -.0667373:
     Y(16) = -.047204.

310  Y(17) = -.0295912: Y(18)= -.0140620: Y(19)= -.0006752.

320  Y(20) = -.010583: Y(21) = .019804: Y(22)= 0.027107
     Y(23) = .0326383.

330  Y(24) = .0365665: Y(25)= .029067: Y(26)= 0.0403226:
     Y(27) = 0.0405085.

340  Y(28) = .0397995: Y(29)= .0383604: Y(30)= 0.0363451:
     Y(31) = .0338961.

350  Y(32) = .0311420: Y(33)= .0281976: Y(34)= 0.251629:
     Y(35) = .0221241.

360  Y(36) = .019153: Y(37)= .0163071: Y(38)= .036326:
     Y(39) = .0111631

370  Y(40) = .0089212: Y(41)= .0069205: Y(42)= .0051654:
     Y(43) = .0036545.
380  Y(44) = .0023793: Y(45)= .0013268: Y(46)= .0004807:
     Y(47) = -.0001781.
```

```
390  Y(48) = -.00067: Y(49)= -.0010167: Y(50)= -.0012393:
     Y(51) = -.001358

400  Y(52) = -.0013942: Y(53)= -.0013645: Y(54)= -.0012859.
410  Y(55) = -.0011729: Y(56)= -.0010382: Y(57)= -.0008923
420  Y(58) = -.0007437: Y(59)= -.0005993: Y(60)= -.0004642
430  Y(61) = -.0003418: Y(62)= -.0002343: Y(63)= -.0001429
440  Y(64) = -.0000678: Y(65)= -.0000083: Y(66)= .0000366
450  Y(67) = .0000683: Y(68)= .0000887: Y(69)= .0000996:
     Y(70) = .0001026.

460  Y(71) = .0000997: Y(72)= .0000925: Y(73)= .0000822:
     Y(74) = .0000703

470  Y(75) = .0000577: Y(76)= .0000452
480  Y(77) = .0000335: Y(78) = .0000230: Y(79)= .0000139:
     Y(80) = .0000063:

490  Y(81) = .0000004
500  S1 = 6.01: S2 = 21 31
502  E2=56: J2=1: X7=0: E1=2.4414E-6
503  E3=105: E4=165: E5=237: E6=393: E7=489: E8=681:
     E9=1065
509  FOR F = 1 TO 10 50 30
510  X7 = E1 * I
511  X8 = 100000* X7
512  T(I) = LN(X8)
```

```
513  PR. T(I), B(8,0,I+E2), J2,I
514  Z(I) = X8 * B(8,0,I+E2)
515  J2 = J2+1
517  NEXTI
518  PR.I,J2
520  X7 = E1 * J2
525  X8 = 100000 * X7
530  T(I) = LN(X8)
532  PR.T(I), B(8,0,E2+J2),J2,I
535  Z(I) = X8 * B(8,0,E2 + J2)
540  I = I+1
542  IF J2+E2 < E3 GO TO 580
545  IF J2 + E2<E4 GO TO 590
547  IF J2+E2 < E5 GO TO 600
548  IF J2+E2 < E6 GO TO 610
550  IF J2+E2 < E7 GO TO 620
560  IF J2+E2 < E8 GO TO 630
565  IF J2+E2 < E9 GO TO 640
570  GO TO 650
580  J2 = J2+2: GO TO 520
590  J2= J2+4 : GO TO 520
600  J2 = J2+6: GO TO 520
610  J2 = J2+8: GO TO 520
620  J2 = J2+16: GO TO 520
```

```
630  J2 = J2+32 : GO TO 520
640  J2 = J2+64 : GO TO 520
650  P1 = I-1
660  PR. 'P1', P1
670  U = 0: C1 = 1: M=4
680  CHAIN 31
```

File 31:

```
 10  REM ****************************
 20  REM CONTINUATION FOR MAIN PROGRAM
 30  REM ****************************
 35  DIM D(225), E(225)
 37  DIM V(100), F(100), G(100), C(100)
 38  PR. U . U
 40  FOR J = 1 TO P1
 50  T3 = Cos(U*T(J)) : T4 = Sin(U*T(J))
 60  D(J) = T3*Z(J): E(J) = T4*Z(J)
 70  NEXT J
 80  B(2,0,C1) = U
 90  GOSUB 370
 91  S3 = S5
 92  FOR J9 = 1 TO P1
 94  D(J9) = E(J9)
 96  NEXT J9
100  GOBUS 370
105  S4 = S5
```

```
110  C(C1) = S3*(1/(SQR(2*PI)))
120  F(C1) = S4*(1/(SQR (2*PI)))
130  U = U + 0.1
140  C1 = C1+1
150  IF U < S1 GO TO 40
160  FOR K=1 TO S2
170  D3 = X(K): D4 = Y(K)
180  I2 = ((X(K)) * (X(K))+(Y(K))*(Y(K)))
190  G(K) = ((C(K)*D3) + (F(K)*D4))/I2
200  V(K) = ((F(K) * D3) - (C(K)*D4))/I2
210  NEXT K
220  Y1 = 0: Y2 = 1
222  PR. 'MU', S2/10
225  PR. 'Y', Y1
230  FOR L = 1 TO S2
240  Y6 = COS (Y1 * B(2,0,L))
250  Y7 = SIN (Y1 * B(2,0,L))
260  P4 = Y6 * G(L): P5 = Y7 * V(L)
270  D(L) = (P4+P5)
275  T(L) = B(2,0,L)
280  NEXT L
285  P1 = S2
290  GO SUB 370
300  X9 = (SQR (2/PI)) * S5
305  B(M,0,Y2) = X9/100000
310  X8 = EXP (-Y1)
```

```
312  B(7,0,Y2) = X8
315  PR. X8, X9/100000
320  Y1 = Y1+0.1: Y2 = Y2+1
330  IF Y1 < = .01 GO TO 225
340  S2 = S2 + 20
350  IF S2 >=62 GO TO 363
355  M = M+1 : PR. 'M', M
360  GO TO 220
363  STOP
370  REM **********************
380  REM NUMERICAL/INTEGRATION ROUTINE
390  REM ****************************
400  E5=0: 05=0
405  PR. 'P1', P1
410  J5 = 2: P5 = P1-1:N=1
420  D8 = T(J5+1) -T(J5)
430  F5 = D(1) + D(P1)
440  IF N=(INT(N/2))*2 GO TO 470
450  05 = 05+D(J5)
460  GO TO 480
470  E5=E5+D(J5)
480  J5=J5+1: N=N+1
490  IF J5<=P5 GO TO 440
500  S5 = (F5+2*E5+4*05)*(D8/3.0)
510  PR. 'INT', S5
520  RETURN
```

APPENDIX III

This briefly explains the various quantities, which are shown in each of the plots given in the various chapters. A plot can display a single waveform as shown in Fig. 5.6(a) or (b). Or display two waveforms one superimposed upon the other as in Fig. 5.2(a) or (b) or two waveforms, in which there is one displayed above and other below as depicted in Fig. 5.8(a) or (b). In the case where only a single waveform is shown, the values are displayed above the plot and where more two waveforms are used, the quantities pertaining to both are separately shown, one above the plot and other below the plot. The values of these quantities are shown with the help of a cursor and in the plots, the this is the third line For illustration, a typical plot in Fig. A is given, showing two waveforms, one above and other below. The plot atthe right, in particular, is chosen and the description f each of the quantities is given. The six quantities above this plot refer to the upper signal waveform and three quant ties below the plot show the values for lower waveform. Thc description of these is as follows:

a : This refers to the analysis operation done to get the waveform. In our case, since averaging was done to ge cleaner singal, acquired in channel 1, therefore 'CH1 AVERAGE' is printed in that place.

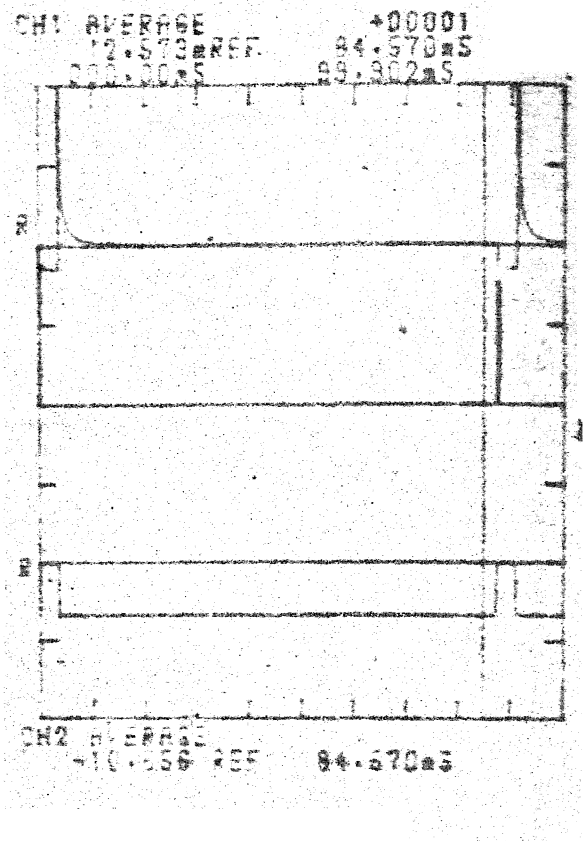
CH1 AVERAGE
+00001
12.573mREF
84.570mS
CH2 AVERAGE
84.570mS

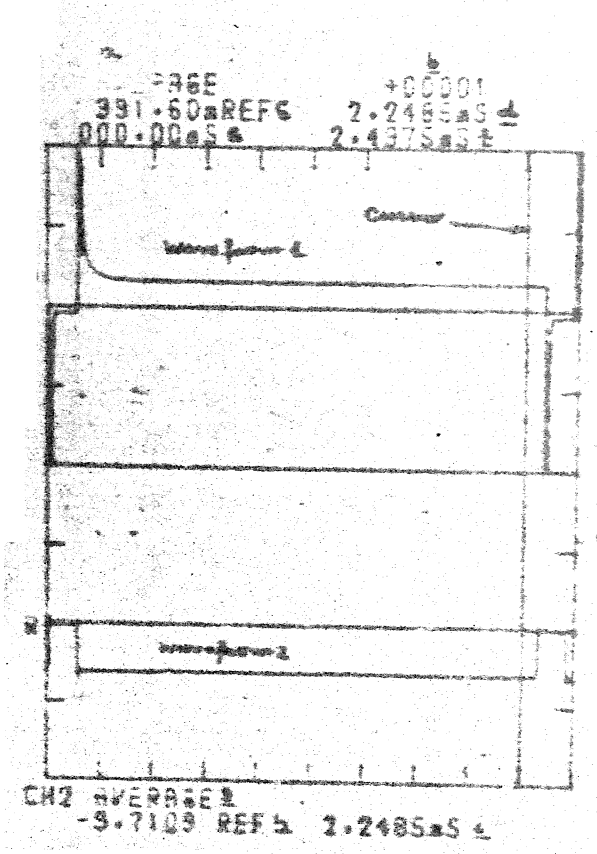
+00001
391.60mREF
2.2485mS
CH2 AVERAGE
-9.7109 REF
2.2485mS

Fig. A

b : This gives the number of such averagings done to get the two waveforms.

c : This refers to the amplitude of the waveform at the point where cursor is placed. This is seen to be 391.60 m REF or mV.

d : This refers to the time instant on the waveform at which the cursor refers to the value in c.

e : This gives the starting time instant of the plot and always shows it as 000.00 msec.

f : This gives the total time to which the signal acquired is displayed. Thus '2.4975 ms' means that signals shown are only upto that time instant.

g : This pertains to the lower second signal, which was acquired in channel 2 through averaging operation. Hence the name 'CH2 AVERAGE' .

h : This gives the amplitude of the lower waveform at the cursor point.

i : The time instant at which the value of h is given is displayed in this.

This completes our description of the plots.

BIBLIOGRAPHY

1. Sohrab K. Gandhi, 'The theory and practice of micro-electronics', John Wiley and Sons, 1968.

2. P. Braunlich Ed., 'Thermally stimulated relaxation in solids', vol. 37, Springer Verlag, 1979.

3. C.T. Sah, L. Forbes, L.L. Rosier and A.F. Tasch Jr., 'Thermal and optical emission and capture rates and cross-sections of electrons and holes at imperfection centers in semiconductors from photo and dark junction current and capacitance experiments', Solid State Electronics, vol. 13, pp. 759-788, 1970.

4. Judith A., Borsuk and Richard. M. Swanson, 'Current Transient spectroscopy: A high sensitivity DLTS system', IEEE Trans. on Electron Devices, vol. ED-27, No. 12, pp. 2217-2225, Dec. 1980.

5. Lang D.V., 'Deep level transient spectroscopy: A new method to characterize traps in semiconductors', Jr. of Appl. Physics, vol. 45, No. 7, pp. 3023-3032, July,1974.

6. White A.M., B. Day and A.J. Grant, 'The effect of non-exponential transients on determination of deep level activation energies by DLTS', Journal of Physics 'C', vol. 12, pp. 4833-38, 1979.

7. L.F. Eastman, Kirchner P.D., W.J. Schaff and G.N. Marcas, 'The analysis of exponential and nonexponential transients in DLTS', Journal of Appl. Physics, vol. 52, pp. 6462-6470, Nov. 1981.

8. Wagner E.L., Don Hiller and Dan E. Mars, 'Fast digital apparatus for capacitance transient analysis', Review Scientific Instruments, vol. 51(9), pp. 1205-1211, Sept. 1980.

9. W.M. Bullis, 'Properties of Gold in Silicon', Solid State Electronics, vol. 9(2), pp. 143-168, 1966.

10. D.V. Lang, H.G. Grimmeiss, E. Meijer and M. Jaras, 'Complex nature of Gold related deep levels in silicon', Physics Rev. 'B', vol. 22, No. 7, Oct. 1980.

11. Lanczos C., 'Applied Analysis', Prentice Hall Inc. 196

12. Gardner J.G., J.C. Gardner, G. Laush and W.W. Meinke, 'Method for the analysis of multi-component exponential decay curves', Journal of Chem. Physics, vol. 3, No. 4, Oct. 1959.

13. Bosshart W.C., 'Printed Circuits Boards, CEDT', Tata McGrawhill.

14. Krishnan K.S., 'Waveform Processor based current transient spectroscopy', M.Tech. thesis, IIT Kanpur, 1983.

15. Abramov A.A., 'Tables of ln [Z] for complex argument', Pergaman Press, 1960.

16. Wu and Peaker, 'Capture cross-sections of the Gold donor and acceptor states in n-type Czochalski silicon' Solid state Electrons, vol. 25, No. 7, pp. 643-649, 1982.

A 84237

EE-1984-M-RAZ-STU